26

Finite Element Templates for Plate Bending

TABLE OF CONTENTS

		Page
§26.1.	**Introduction**	26–3
§26.2.	**High Performance Elements**	26–4
	§26.2.1. Tools for Construction of HP Elements	26–5
	§26.2.2. Unification by Parametrized Variational Principles	26–5
§26.3.	**Finite Element Templates**	26–6
	§26.3.1. The Fundamental Decomposition	26–7
	§26.3.2. Constructing the Component Stiffness Matrices	26–8
	§26.3.3. Basic Stiffness Properties	26–8
	§26.3.4. Constructing Optimal Elements	26–9
§26.4.	**Templates for 3-Node KPT Elements**	26–9
	§26.4.1. Stiffness Decomposition	26–9
	§26.4.2. The KPT-1-36 and KPT-1-9 Templates	26–10
	§26.4.3. Element Families	26–11
	§26.4.4. Template Genetics: Signatures and Clones	26–11
	§26.4.5. Parameter Constraints	26–13
	§26.4.6. Staged Element Design	26–13
§26.5.	**Linear Constraints**	26–14
	§26.5.1. Observer Invariance (OI) Constraints	26–14
	§26.5.2. Aspect Ratio Insensitivity (ARI) Constraints	26–14
	§26.5.3. Energy Orthogonality (ENO) Constraints	26–16
§26.6.	**Quadratic Constraints**	26–17
	§26.6.1. Morphing Constraints	26–17
	§26.6.2. Mesh Direction Insensitivity Constraints	26–18
	§26.6.3. Distortion Minimization Constraints	26–19
§26.7.	**New KPT Elements**	26–20
§26.8.	**Benchmark Studies**	26–21
	§26.8.1. Simply Supported and Clamped Square Plates	26–21
	§26.8.2. Uniformly Loaded Cantilever	26–22
	§26.8.3. Aspect Ratio Test of End Loaded Cantilever	26–22
	§26.8.4. Aspect Ratio Test of Twisted Ribbon	26–23
	§26.8.5. The Score so Far	26–24
§26.9.	**Concluding Remarks**	26–25
§26.	**References**	26–25
§26.A.	**Formulation of KPT-1-36 Template**	26–27
§26.A.1.	**Element Relations**	26–27
§26.A.2.	**The Basic Stiffness Template**	26–28
§26.A.3.	**The Higher Order Stiffness Template**	26–29

Material below appeared as: C. A. Felippa, Recent advances in finite element templates, Chapter 4 in *Computational Mechanics for the Twenty-First Century*, ed. by B.H.V. Topping, Saxe-Coburn Publications, Edinburgh, 71–98, 2000.

RECENT ADVANCES IN FINITE ELEMENT TEMPLATES

Carlos A. Felippa

Department of Aerospace Engineering Sciences
and Center for Aerospace Structures
University of Colorado at Boulder
Boulder, Colorado 80309-0429, USA

Abstract: A finite element template is a parametrized algebraic form that reduces to specific finite elements by setting numerical values to the free parameters. Following an outline of high performance elements, templates for Kirchhoff Plate-Bending Triangles (KPT) with 3 nodes and 9 degrees of freedom are studied. A 37-parameter template is constructed using the Assumed Natural Deviatoric Strain (ANDES) approach. Specialization of this template includes well known elements such as DKT and HCT. The question addressed here is: can these parameters be selected to produce high performance elements? The study is carried out by staged application of constraints on the free parameters. The first stage produces element families satisfying invariance and aspect ratio insensitivity conditions. Application of energy balance constraints produces specific elements. The performance of such elements in a preliminary set of benchmark tests is reported.

Special Lecture presented to the Fifth International Conference on Computational Structures Technology, 6-8 September 2000, Leuven, Belgium. Published as Chapter 4 in *Computational Mechanics for the Twenty-First Century*, ed. by B.H.V. Topping, Saxe-Coburn Publications, Edinburgh, 71–98, 2000.

§26.1. Introduction

The Finite Element Method (FEM) was first described in the presently dominant form by Turner et. al. [1]. It was baptized by Clough [2] at the beginning of an explosive growth period. The first applications book, by Zienkiewicz and Cheung [3] appeared seven years later. The first monograph on the mathematical foundations was written by Strang and Fix [4]. The opening sentence of this book already declared the FEM an "astonishing success." And indeed the method had by then revolutionized computational structural mechanics and was in its way to impact non-structural applications.

The FEM was indeed the right idea at the right time. The key reinforcing factor was the expanding availability of digital computers. Lack of this enabling tool meant that earlier related proposals, notably that of Courant [5], had been forgotten. A second enabler was the heritage of classical structural mechanics and its reformulation in matrix form, which culminated in the elegant unification of Argyris

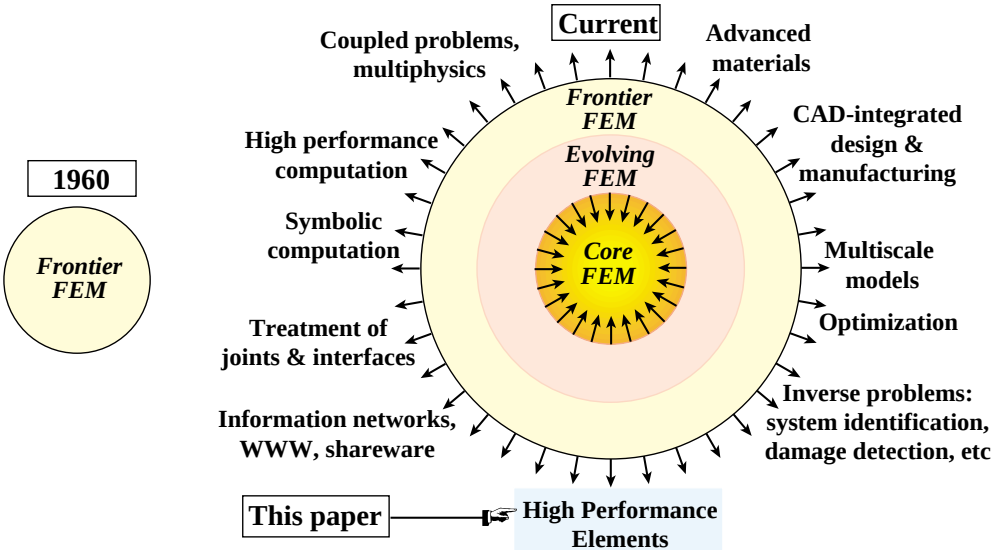

FIGURE 26.1. Evolution of the Finite Element Method.

and Kelsey [6]. A third influence was the victory of the Direct Stiffness Method (DSM) developed by Turner [7,8] over the venerable Force Method, a struggle recently chronicled by Felippa [9]. Victory was sealed by the adoption of the DSM in the earlier general-purpose FEM codes, notably NASTRAN, MARC and SAP. In the meantime the mathematical foundations were rapidly developed in the 1970s.

"Astonishing success", however, carries its own dangers. By the early 1980s the FEM began to be regarded as "mature technology" by US funding agencies. By now that feeling has hardened to the point that it is virtually impossible to get significant research support for fundamental work in FEM. This viewpoint has been reinforced by major software developers, which proclaim their products as solutions to all user needs.

Is this perception correct? It certainly applies to the *core FEM*, or orthodox FEM. This is the material taught in textbooks and which is implemented in major software products. Core FEM follows what may be called the Ritz-Galerkin and Direct Stiffness Method canon. Beyond the core there is an *evolving FEM*. This is strongly rooted on the core but goes beyond textbooks. Finally there is a *frontier FEM*, which makes only partial or spotty use of core knowledge. See Figure 26.1.

By definition core FEM is mature. As time goes, it captures segments of the evolving FEM. For example, most of the topic of FEM mesh adaptivity can be classified as evolving, but will eventually become part of the core. Frontier FEM, on the other hand, can evolve unpredictably. Some components prosper, mature and eventually join the core, some survive but never become orthodox, while others wither and die.

Four brilliant contributions of Bruce Irons, all of which were frontier material when first published, can be cited as examples of the three outcomes. *Isoparametric elements* and *frontal solvers* rapidly became integral part of the core technology. The *patch test* has not become part of the core, but survives as a useful if controversial tool for element development and testing. The *semi-loof shell elements* quietly disappeared.

Topics that drive frontier FEM include multiphysics, multiscale models, symbolic and high performance computation, integrated design and manufacturing, advances in information technology, optimization, inverse problems, materials, treatment of joints and interfaces, and high performance elements. This paper deals with the last topic.

§26.2. High Performance Elements

An important area of frontier FEM is the construction of high performance (HP) finite elements. These were defined by Felippa and Militello [10] as "simple elements that deliver engineering accuracy with arbitrary coarse meshes." Some of these terms require clarification.

Simple means the simplest geometry and freedom configuration that fits the problem and target accuracy consistent with human and computer resources. This can be summed up in one FEM modeling rule: *use the simplest element that will do the job*.

Engineering accuracy is that generally expected in most FEM applications in Aerospace, Civil and Mechanical Engineering. Typically this is 1% in displacements and 10% in strains, stresses and derived quantities. Some applications, notably in Aerospace, require higher precision in quantities such as natural frequencies, shape tolerances, or in long-time simulations.

Coarse mesh is one that suffices to capture the important physics in terms of geometry, material and load properties. It does not imply few elements. For example, a coarse mesh for a fighter aircraft undergoing maneuvers may require several million elements. For simple benchmark problems such as a uniformly loaded square plate, a mesh of 4 or 16 elements may be classified as coarse.

Finally, *arbitrary mesh* implies *low sensitivity to skewness and distortion*. This attribute is becoming important as push-button mesh generators gain importance, because generated meshes can be of low quality compared to those produced by an experienced analyst.

For practical reasons we are interested only in the construction of HP elements with *displacement* nodal degrees of freedom. Such elements are characterized by their stiffness equations, and thus can be plugged into any standard finite element program.

§26.2.1. Tools for Construction of HP Elements

The origins of HP finite elements may be traced to several investigators in the late 1960s and early 1970s. Notable early contributions are those of Clough, Irons, Taylor, Wilson and their coworkers. The construction techniques made use of incompatible shape functions, the patch test, reduced, selective and directional integration. These can be collectively categorized as unorthodox, and in fact were labeled as "variational crimes" at that time by Strang and Fix [4].

A more conventional development, pioneered by Pian, Tong and coworkers, made use of mixed and hybrid variational principles. They developed elements using stress or partial stress assumptions, but the end product were standard displacement elements. These techniques were further refined in the 1980s. A good expository summary is provided in the book by Zienkiewicz and Taylor [11].

New innovative approaches came into existence in the 1980s. The most notable have been the Free Formulation of Bergan and Nygård [12,13], and the Assumed Strain method pioneered by MacNeal [14]. The latter was further developed along different paths by Bathe and Dvorkin [15], Park and Stanley [16], and Simo and Hughes [17].

§26.2.2. Unification by Parametrized Variational Principles

The approach taken by the author started from collaborative work with Bergan in Free Formulation (FF) high performance elements. The results of this collaboration were a membrane triangle with drilling freedoms described in Bergan and Felippa [18] and a plate bending triangle presented by Felippa and Bergan [19]. It continued with exploratory work using the Assumed Natural Strain (ANS) method of Park and Stanley [16]. Eventually FF and ANS coalesced in a variant of ANS called Assumed

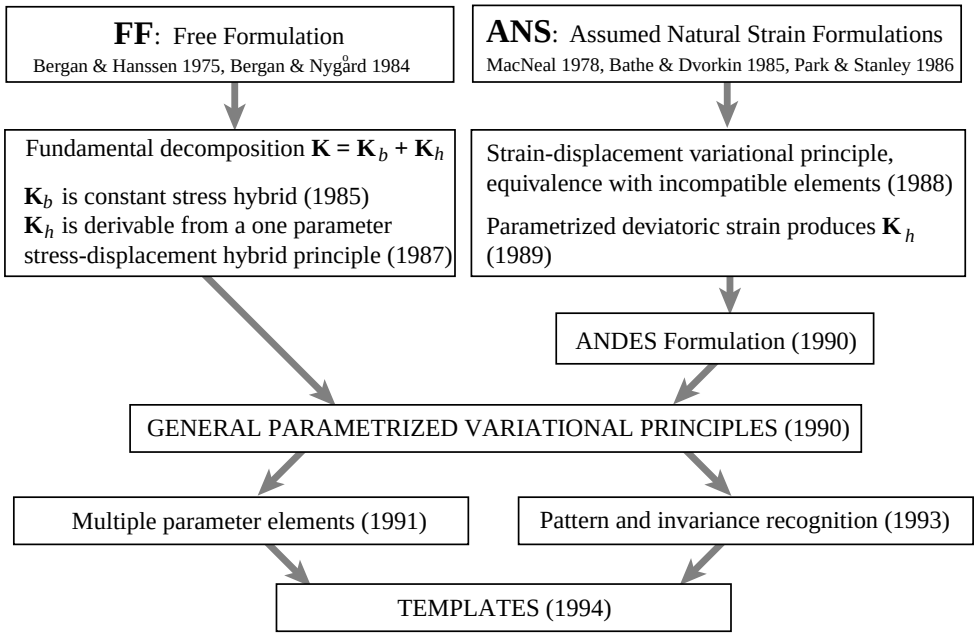

FIGURE 26.2. The road to templates.

Natural Deviatoric Strain, or ANDES. High performance elements based on the ANDES formulation are described by Militello and Felippa [20] and Felippa and Militello [21].

This unification work led naturally to a formulation of elasticity functionals containing free parameters. These were called parametrized variational principles, or PVPs in short. Setting the parameters to specific numerical values produced the classical functionals of elasticity such as Total Potential Energy, Hellinger-Reissner and Hu-Washizu. For linear elasticity, three free parameters in a three-field functional with independently varied displacements, strains and stresses are sufficient to embed all classical functionals. Two survey articles with references to the original papers are available [22,23].

One result from the PVP formulation is that, upon FEM discretization, free parameters appear at the element level. One thus naturally obtains *families* of elements. Setting the free parameters to numerical values produces specific elements. Although the PVP Euler-Lagrange equations are the same excepts for weights, the discrete solution produced by different elements are not. Thus an obvious question arises: which free parameters produce the best elements? It turns out that there is no clear answer to the question, because the best set of parameters depends on the element geometry. Hence the equivalent question: which is the best variational principle? makes no sense.

The PVP formulation led, however, to an unexpected discovery. The configuration of elements constructed according to PVPs and the usual assumptions on displacements, stresses and strains was observed to follow specific algebraic rules. *Such configurations could be parametrized directly without going through the source PVP*. This observation led to a general formulation of finite elements as *templates*.

The aforementioned developments are flowcharted in Figure 26.2.

§26.3. Finite Element Templates

A finite element template, or simply *template*, is an algebraic form that represents element-level stiffness equations, and which fulfills the following conditions:

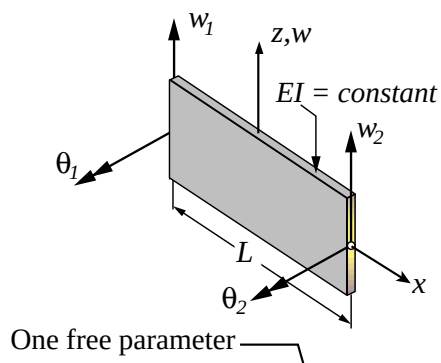

$$\mathbf{K} = \mathbf{K}_b + \mathbf{K}_h = \frac{EI}{L}\begin{bmatrix} 0 & 0 & 0 & 0 \\ 0 & 1 & 0 & -1 \\ 0 & 0 & 0 & 0 \\ 0 & -1 & 0 & 1 \end{bmatrix} + \boxed{\beta}\frac{EI}{L^3}\begin{bmatrix} 4 & -2L & -4 & -2L \\ -2L & L^2 & 2L & L^2 \\ -4 & 2L & 4 & 2L \\ -2L & L^2 & 2L & L^2 \end{bmatrix}$$

FIGURE 26.3. Template for Bernoulli-Euler prismatic plane beam.

(C) Consistency: the Individual Element Test (IET) form of the patch test, introduced by Bergan and Hanssen [24], is passed for any element geometry.

(S) Stability: the stiffness matrix satisfies correct rank and nonnegativity conditions.

(P) Parametrization: the element stiffness equations contain free parameters.

(I) Invariance: the element equations are observer invariant. In particular, they are independent of node numbering and choice of reference systems.

The first two conditions: (C) and (S), are imposed to ensure convergence. Property (P) permits performance optimization as well as tuning elements to specific needs. Property (I) helps predictability and benchmark testing.

Setting the free parameters to numeric values yields specific element instances.

§26.3.1. The Fundamental Decomposition

A stiffness matrix derived through the template approach has the fundamental decomposition

$$\mathbf{K} = \mathbf{K}_b(\alpha_i) + \mathbf{K}_h(\beta_j) \tag{26.1}$$

Here $\mathbf{K}_b$ and $\mathbf{K}_h$ are the basic and higher-order stiffness matrices, respectively. The basic stiffness matrix $\mathbf{K}_b$ is constructed for *consistency* and *mixability*, whereas the higher order stiffness $\mathbf{K}_h$ is constructed for *stability* (meaning rank sufficiency and nonnegativity) and *accuracy*. As further discussed below, the higher order stiffness $\mathbf{K}_h$ must be orthogonal to all rigid-body and constant-strain (curvature) modes.

In general both matrices contain free parameters. The number of parameters α_i in the basic stiffness is typically small for simple elements. For example, in the 3-node, 9-DOF KPT elements considered here there is only one basic parameter, called α. This number must be the *same for all elements in a mesh* to insure satisfaction of the IET [18].

On the other hand, the number of higher order parameters β_j can be in principle *infinite* if certain components of $\mathbf{K}_h$ can be represented as a polynomial series of element geometrical invariants. In practice, however, such series are truncated, leading to a finite number of β_j parameters. Although the

β_j may vary from element to element without impairing convergence, often the same parameters are retained for all elements.

As an illustration Figure 26.3 displays the template of a simple one-dimensional element: a 2-node, 4-DOF plane Bernoulli-Euler prismatic beam. This has only one free parameter: β, which scales the higher order stiffness. A simple calculation [22] shows that its optimal value is $\beta = 3$, which yields the well-known Hermitian beam stiffness. This is known as a *universal template* since it include all possible beam elements that satisfy the foregoing conditions.

§26.3.2. Constructing the Component Stiffness Matrices

The basic stiffness that satisfies condition (C) is the same for any formulation. It is simply a constant stress hybrid element [13,18]. For a specific element and freedom configuration, $\mathbf{K}_b$ can be constructed once and for all.

The formulation of the higher order stiffness $\mathbf{K}_h$ is not so clear-cut, as can be expected because of the larger number of free parameters. It can be done by a variety of techniques, which are summarized in a article by Felippa, Haugen and Militello [25]. Of these, one has proven exceedingly useful for the construction of templates: the ANDES formulation. ANDES stands for Assumed Natural DEviatoric Strains. It is based on assuming natural strains for the high order stiffness. For plate bending (as well as beams and shells) natural curvatures take the place of strains.

Second in usefulness is the Assumed Natural DEviatoric STRESSes or ANDESTRESS formulation, which for bending elements reduces to assuming deviatoric moments. This technique, which leads to stiffness templates that contain inverses of natural flexibilities, is not considered here.

§26.3.3. Basic Stiffness Properties

The following properties of the template stiffness equations are collected here for further use. They are discussed in more detail in the article by Felippa, Haugen and Militello [25]. Consider a test displacement field, which for thin plate bending will be a continuous transverse displacement mode $w(x, y)$. [In practical computations this will be a polynomial in x and y.] Evaluate this at the nodes to form the element node displacements $\mathbf{u}$. These can be decomposed into

$$\mathbf{u} = \mathbf{u}_b + \mathbf{u}_h = \mathbf{u}_r + \mathbf{u}_c + \mathbf{u}_h, \tag{26.2}$$

where $\mathbf{u}_r$, $\mathbf{u}_c$ and $\mathbf{u}_h$ are rigid body, constant strain and higher order components, respectively, of $\mathbf{u}$. The first two are collectively identified as the *basic* component $\mathbf{u}_b$. The matrices (26.1) must satisfy the stiffness orthogonality conditions

$$\mathbf{K}_b\mathbf{u}_r = \mathbf{0}, \quad \mathbf{K}_h\mathbf{u}_r = \mathbf{0}, \quad \mathbf{K}_h\mathbf{u}_c = \mathbf{0} \tag{26.3}$$

while $\mathbf{K}_b$ represents exactly the response to $\mathbf{u}_c$.

The strain energy taken up by the element under application of $\mathbf{u}$ is $U = \frac{1}{2}\mathbf{u}^T\mathbf{K}\mathbf{u}$. Decomposing $\mathbf{K}$ and $\mathbf{u}$ as per (26.1) and (26.2), respectively, and enforcing (26.3) yields

$$U = \tfrac{1}{2}(\mathbf{u}_b + \mathbf{u}_h)^T\mathbf{K}_b(\mathbf{u}_b + \mathbf{u}_h) + \tfrac{1}{2}\mathbf{u}_h^T\mathbf{K}_h\mathbf{u}_h = U_b + U_h \tag{26.4}$$

U_b and U_h are called the basic and higher order energy, respectively. Let U_{ex} be the exact energy taken up by the element as a continuum body subjected to the test displacement field. The element energy ratios are defined as

$$\rho = \frac{U}{U_{ex}} = \rho_b + \rho_h, \quad \rho_b = \frac{U_b}{U_{ex}}, \quad \rho_h = \frac{U_h}{U_{ex}}. \tag{26.5}$$

Here ρ_b and ρ_h are called the basic and higher order energy ratios, respectively. If $\mathbf{u}_h = \mathbf{0}$, $\rho = \rho_b = 1$ because the element must respond exactly to any basic mode by construction. For a general displacement mode in which $\mathbf{u}_h$ does not vanish, ρ_b is a function of the α_i whereas ρ_h is a function of the β_j.

§26.3.4. Constructing Optimal Elements

By making a template sufficiently general all published finite elements for a specific configuration can be generated. This includes those derivable by orthodox techniques (for example, shape functions) and those that are not. Furthermore, an infinite number of new elements arise. The same question previously posed for PVPs arises: Can one select the free parameters to produce an optimal element?

The answer is not yet known for general elements. The main unresolved difficulty is: which optimality conditions must be imposed at the local (element) level? While some of them are obvious, for example those requiring observer invariance, most of the others are not. The problem is that *a detailed connection between local and global optimality is not fully resolved by conventional FEM error analysis*. Such analysis can only provide convergence rates expressed as $C\,h^m$ in some error norm, where h is a characteristic mesh dimension and m is usually the same for all template instances. The key to high performance is the coefficient C, but this is problem dependent. Consequently, verification benchmarks are still inevitable.

As noted, conventional error analysis is of limited value because it only provides the exponent m, which is typically the *same* for all elements in a template. It follows that several template optimization constraints discussed later are heuristic. But even if the local-to-global connection were fully resolved, a second technical difficulty arises: the actual construction and optimization of templates poses formidable problems in symbolic matrix manipulation, because one has to carry along arbitrary geometries, materials and free parameters.

Until recently those manipulations were beyond the scope of computer algebra systems (CAS) for all but the simplest elements. As personal computers and workstations gain in CPU speed and storage, it is gradually becoming possible to process two-dimensional elements for plane stress and plate bending. Most three-dimensional and curved-shell elements, however, still lie beyond the power of present systems.

Practitioners of optimization are familiar with the dangers of excessive perfection. A system tuned to operate optimally for a narrow set of conditions often degrades rapidly under deviation from such conditions. The benchmarks of Section 8 show that a similar difficulty exists in the construction of optimal plate elements, and that expectations of an "element for all seasons" must be tempered.

§26.4. Templates for 3-Node KPT Elements

The application of the template approach is rendered specific by studying a particular configuration: a 3-node flat triangular element to model bending of Kirchhoff (thin) plates. The element has the conventional 3 degrees of freedom: one transverse displacement and three rotations at each corner, as illustrated in Figure 26.4.

For brevity this will be referred to as a Kirchhoff Plate Triangle, or KPT, in the sequel. The complete development of the template is given in the Appendix. In the following sections we summarize only the important results necessary for the application of local optimality constraints.

§26.4.1. Stiffness Decomposition

For the KPT elements under study the configuration of the stiffness matrices in (26.1) can be shown in more detail. Assuming that the 3×3 moment-curvature plate constitutive matrix $\mathbf{D}$ is constant over the

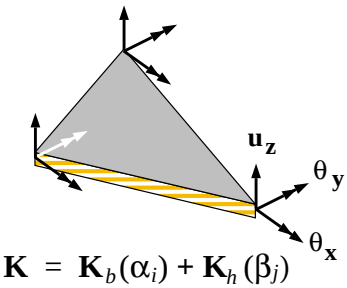

$$\mathbf{K} = \mathbf{K}_b(\alpha_i) + \mathbf{K}_h(\beta_j)$$

Template name											
KPT-1-9	element-acronym	α	β_{10}	β_{20}	β_{30}	β_{40}	β_{50}	β_{60}	β_{70}	β_{80}	β_{90}
KPT-1-36	element-acronym	α	β_{10}	β_{20}	β_{30}	β_{40}	β_{50}	β_{60}	β_{70}	β_{80}	β_{90}
			β_{11}	β_{21}	β_{31}	β_{41}	β_{51}	β_{61}	β_{71}	β_{81}	β_{92}
			β_{12}	β_{22}	β_{32}	β_{42}	β_{52}	β_{62}	β_{72}	β_{82}	β_{93}
			β_{13}	β_{23}	β_{33}	β_{43}	β_{53}	β_{63}	β_{73}	β_{83}	β_{93}

Template signatures

FIGURE 26.4. Template for Kirchhoff plate-bending triangles (KPT) studied here.

triangle, we have

$$\mathbf{K}_b = \frac{1}{A}\mathbf{L}\mathbf{D}\mathbf{L}^T, \quad \mathbf{K}_h = \frac{A}{3}\left[\mathbf{B}_{\chi 4}^T\mathbf{D}_\chi\mathbf{B}_{\chi 4} + \mathbf{B}_{\chi 5}^T\mathbf{D}_\chi\mathbf{B}_{\chi 5} + \mathbf{B}_{\chi 6}^T\mathbf{D}_\chi\mathbf{B}_{\chi 6}\right]. \tag{26.6}$$

Here A is the triangle area, $\mathbf{L}$ is the 9×3 force lumping matrix that transforms a constant internal moment field to node forces, $\mathbf{B}_{\chi m}$ are 3×9 matrices relating natural curvatures at triangle midpoints $m = 4, 5, 6$ to node displacements, and $\mathbf{D}\chi$ is the plate constitutive matrix transformed to relate natural curvatures to natural moments. Parameter α appears in $\mathbf{L}$ whereas parameters β_j appear in $\mathbf{B}_{\chi m}$. Full expressions of these matrices are given in the Appendix.

§26.4.2. The KPT-1-36 and KPT-1-9 Templates

A useful KPT template is based on a 36-parameter representation of $\mathbf{K}_h$ in which the series noted above retains up to the *linear* terms in three triangle geometric invariants λ_1, λ_2 and λ_3, defined in the Appendix, which characterize the deviations from the equilateral-triangle shape. The template is said to be of *order one* in the λs. It has a total of 37 free parameters: one α and 36 βs. Collectively this template is identified as KPT-1-36. Instances are displayed using the following tabular arrangement:

acronym	α	β_{10}	β_{20}	β_{30}	β_{40}	β_{50}	β_{60}	β_{70}	β_{80}	β_{90}	$/\beta_{sc}$
		β_{11}	β_{21}	β_{31}	β_{41}	β_{51}	β_{61}	β_{71}	β_{81}	β_{91}	
		β_{12}	β_{22}	β_{32}	β_{42}	β_{52}	β_{62}	β_{72}	β_{82}	β_{92}	
		β_{13}	β_{23}	β_{33}	β_{43}	β_{53}	β_{63}	β_{73}	β_{83}	β_{93}	

(26.7)

Here β_{sc} is a scaling factor by which all displayed β_{ij} must be divided; e.g. in the DKT element listed in Table 26.1 $\beta_{10} = -6/4 = -3/2$ and $\beta_{41} = 4/4 = 1$. If β_{sc} is omitted it is assumed to be one.

Setting the 37 parameters to numeric values yield specific elements, identified by the acronym displayed on the left. Some instances that are interesting on account of practical or historical reasons are collected in Table 26.1. Collectively these represents a tiny subset of the number of published KPT elements, which probably ranges in the hundreds, and is admittedly biased in favor of elements developed by the writer and colleagues. Table 26.2 identifies the acronyms of Table 26.1 correlated with original publications where appropriate.

Table 26.1. Template Signatures of Some Existing KPT Elements

Acronym	α	β_{1j}	β_{2j}	β_{3j}	β_{4j}	β_{5j}	β_{6j}	β_{7j}	β_{8j}	β_{9j}	β_{sc}
ALR	0	−3	0	0	0	0	0	0	3	0	/2
		−6	0	0	0	0	0	0	0	0	
		0	0	0	0	0	0	0	0	0	
		0	0	0	0	0	0	0	−6	0	
AQR0	0	Same βs as AQR1									
AQRBE	$1/\sqrt{2}$	Same βs as AQR1									
AQR1	1	−3	0	0	0	0	0	0	3	0	/2
		−2	0	0	0	0	0	0	0	0	
		0	0	0	0	0	0	0	0	−4	
		0	0	0	0	0	0	0	−2	0	
AVG	0	−3	0	0	0	0	0	0	3	0	/2
BCIZ0	0	−3	1	1	0	0	−1	−1	3	0	/2
BCIZ1	1	−3	0	0	−1	1	0	0	3	0	/2
		0	0	0	2	0	0	2	0	0	
		0	0	−2	0	0	−2	0	0	0	
		0	2	0	0	2	0	0	0	0	
DKT	1	−6	1	1	−2	2	−1	−1	6	0	/4
		0	0	0	4	0	0	−2	0	0	
		0	0	2	0	0	2	0	0	0	
		0	−2	0	0	4	0	0	0	0	
FF0	0	−9	1	1	−2	2	−1	−1	9	0	/6
FF1	1	Same βs as FF0.									
HCT	1	−11	5	0	−2	2	0	−5	11	0	/4
		6	0	0	4	0	0	10	0	0	
		0	0	20	0	0	20	0	0	0	
		0	10	0	0	4	0	0	6	0	

An interesting subclass of (26.7) is that in which the bottom 3 rows vanish: $\beta_{11} = \beta_{12} = \ldots\ \beta_{93} = 0$. This 10-parameter template is said to be of *order zero* because the invariants λ_1, λ_2 and λ_3 do not appear in the higher order stiffness. It is identified as KPT-1-9. For brevity it will be written simply as

acronym	α	β_{10}	β_{20}	β_{30}	β_{40}	β_{50}	β_{60}	β_{70}	β_{80}	β_{90}	$/\beta_{sc}$

(26.8)

omitting the zero entries.

§26.4.3. Element Families

Specializations of (26.7) and (26.8) that still contain free parameters are called *element families*. In such a case the free parameters are usually written as arguments of the acronym. For example, Table 26.4 defines the ARI, or Aspect Ratio Insensitive, family derived in Section 6. ARI has seven free parameters identified as α, β_{10}, β_{20}, β_{30}, γ_0, γ_1 and γ_2. Consequently the template acronym is written ARI(α, β_{10}, β_{20}, β_{30}, γ_0, γ_1, γ_2).

A family whose only free parameter is α is called an α-family. Its instances are called α-variants. In some α families the β coefficients are fixed. For example in the AQR(α) and FF(α) families only α changes. Some practically important instances of those families are shown in Table 26.1. In other α-families the βs are functions of α. For example this happens in the BCIZ(α) family, two instances of which, obtained by setting $\alpha = 0$ and $\alpha = 1$, are shown on Table 26.1.

Table 26.2. Element Identifiers Used in Table 26.1

Acronym	Description
ALR	Assumed Linear Rotation KPT element of Militello and Felippa [20].
AQR1	Assumed Quadratic Rotation KPT element of Militello and Felippa [20].
AQR0	α-variant of AQR1 with $\alpha = 0$.
AQRBE	α-variant of AQR1 with $\alpha = 1/\sqrt{2}$; of interest because it is BME.
AVG	Average curvature KPT element of Militello and Felippa [20].
BCIZ0	Nonconforming element of Bazeley, Cheung, Irons and Zienkiewicz [26] "sanitized" with $\alpha = 0$ as described by Felippa, Haugen and Militello [25]. Historically the first polynomial-based, complete, nonconforming KPT and the motivation for the original (multielement) patch test of Irons. See Section 4.4 for two clones of BCIZ0.
BCIZ1	Variant of above, in which the original BCIZ is sanitized with $\alpha = 1$.
DKT	Discrete Kirchhoff Triangle of Stricklin et al. [30] streamlined by Batoz [31]; see also Bathe, Batoz and Ho [32]
FF0	Free Formulation element of Felippa and Bergan [19].
FF1	α variant of FF0 with $\alpha = 1$.
HCT	Hsieh-Clough-Tocher element presented by Clough and Tocher [33] with curvature field collocated at the 3 midpoints. The original (macroelement) version was the first successful C^1 conforming KPT.

§26.4.4. Template Genetics: Signatures and Clones

An examination of Table 26.1 should convince the reader that template coefficients uniquely define an element once and for all, although the use of author-assigned acronyms is common in the FE literature. The parameter set can be likened to an "element genetic fingerprint" or "element DNA" that makes it a unique object. This set is called the element *signature*.

If signatures were randomly generated, the number of element instances would be of course huge: more precisely ∞^{37} for 37 parameters. But in practice elements are not fabricated at random. Attractors emerge. Some element derivation methods, notably those based on displacement shape functions, tend to "hit" certain signature patterns. The consequence is that the same element may be discovered separately by different authors, often using dissimilar derivation techniques. Such elements will be called *clones*. Cloning seems to be more prevalent among instances of the order-zero KPT-1-9 template (26.8). Some examples discovered in the course of this study are reported.

The first successful nonconforming triangular plate bending element was the original BCIZ [26]. This element, however, does not pass the Individual Element Test (IET), and in fact fails Irons' original patch test for arbitrary mesh patterns. The source of the disease is the basic stiffness. The element can be "sanitized" by removing the infected matrix as described by Felippa, Haugen and Militello [25]. This is replaced by a healthy $\mathbf{K}_b$ with, for example, $\alpha = 0$ or $\alpha = 1$. This transplant operation yields the elements called BCIZ0 and BCIZ1, respectively, in Table 26.1. [These are two instances of the BCIZ(α) family.] Note that BCIZ0 pertains to the KPT-1-9 template.

In the 3rd MAFELAP Conference, Hanssen, Bergan and Syversten [27] reported a nonconforming element which passed the IET and (for the time) was of competitive performance. Construction of its

Table 26.3 - Linear Constraints for KPT-1-36 Template

ARI2:	$\beta_{11} = (2\beta_{10} + \beta_{20} + 3\beta_{30} - 4\beta_{40})/3, \quad \beta_{22} = (8\beta_{20} - 4\beta_{30} + 2\beta_{40})/9$
ARI1:	$\beta_{33} = \beta_{20} - \beta_{30} - \beta_{22}, \quad \beta_{92} = 2\beta_{10} + \beta_{20} + 3\beta_{30} - 4\beta_{40} - \beta_{11}$
ARI1:	$\beta_{23} = -2\beta_{20} + \beta_{22}, \quad \beta_{32} = 2\beta_{30} + \beta_{33}, \quad \beta_{41} = -2\beta_{40} - \beta_{33}$
ARI1:	$\beta_{12} = \beta_{22}, \quad \beta_{93} = \beta_{33}, \quad \beta_{13} = -\beta_{33}, \quad \beta_{82} = \beta_{22}, \quad \beta_{43} = -\beta_{33}$
ARI0:	$\beta_{21} = \beta_{31} = \beta_{42} = \beta_{52} = \beta_{63} = \beta_{73} = 0$
ENO1:	$\beta_{32} = \beta_{23}+\beta_{41}, \ \beta_{92} = 2\beta_{11}-\beta_{12}+\beta_{82}, \ \beta_{13} = \beta_{93}-\beta_{82}, \ \beta_{33} = \beta_{22}+\beta_{43}$
ENO0:	$\beta_{40} = -\beta_{20} - \beta_{30}$
OI1:	$\beta_{51} = \beta_{52} + \beta_{43} - \beta_{42}, \quad \beta_{53} = \beta_{52} - \beta_{42} + \beta_{41}, \quad \beta_{61} = \beta_{63} - \beta_{31} + \beta_{33},$
OI1:	$\beta_{62} = \beta_{63} + \beta_{32} - \beta_{31}, \quad \beta_{71} = \beta_{73} - \beta_{21} + \beta_{23}, \quad \beta_{72} = \beta_{73} - \beta_{21} + \beta_{22},$
OI1:	$\beta_{81} = \beta_{82} - \beta_{12} + \beta_{13}, \quad \beta_{83} = \beta_{82} - \beta_{12} + \beta_{11}, \quad \beta_{91} = \beta_{93}$
OI0:	$\beta_{50} = -\beta_{40}, \quad \beta_{80} = -\beta_{10}, \quad \beta_{60} = -\beta_{30}, \quad \beta_{70} = -\beta_{20}, \quad \beta_{90} = 0$

template signature revealed it to be a clone of BCIZ0. The plate bending part of the TRIC shell element [28] is also a clone of BCIZ0.

An energy orthogonal version of the HBS element was constructed by Nygård in his Ph.D. thesis [29]. Its signature turned out to agree with that of the FF0 element, constructed by Felippa and Bergan [19] with a different set of higher order shape functions.

Clones seem rarer in the realm of the full KPT-1-36 template because of its greater richness. The DKT [30–32] appears to be an exception. Although this popular element is usually constructed by assuming rotation fields, it coalesced with one of the ANDES elements derived by Militello and Felippa [20] by assuming natural deviatoric curvatures. At the time the coalescence was suspected from benchmarks, and later verified by direct examination of stiffness matrices. Using the template formulation such numerical tests can be bypassed, since it is sufficient to compare signatures.

§26.4.5. Parameter Constraints

To construct element families and in the limit, specific elements, constraints on the free parameters must be imposed. One key difficulty, already noted in Section 3.4, emerges. Constraints must be imposed at the *local* level of either an individual element or simple mesh units, but they should lead to high performance behavior at the *global* level. There is as yet no mathematical framework for establishing those connections.

Several constraint types have been used in this and previous work: (1) invariance, (2) skewness and aspect ratio insensitivity, (3) distortion insensitivity, (4) truncation error minimization, (5) energy balance, (6) energy orthogonality, (7) morphing, (8) mesh direction insensitivity. Whereas (1) and (2) have clear physical significance, the effect of the others has to be studied empirically on benchmark problems. Conditions that have produced satisfactory results are discussed below with reference to the KPT template. The reader should be cautioned, however, that these may not represent the final word inasmuch as templates are presently a frontier subject. For convenience the constraints can be divided into linear and nonlinear, the former being independent of constitutive properties.

§26.4.6. Staged Element Design

Taking an existing KPT element that passes the IET and finding its template signature is relatively straightforward with the help of a computer algebra program. Those listed in T Table 26.1 were obtained using *Mathematica*. But in element design we are interested in the reverse process: starting

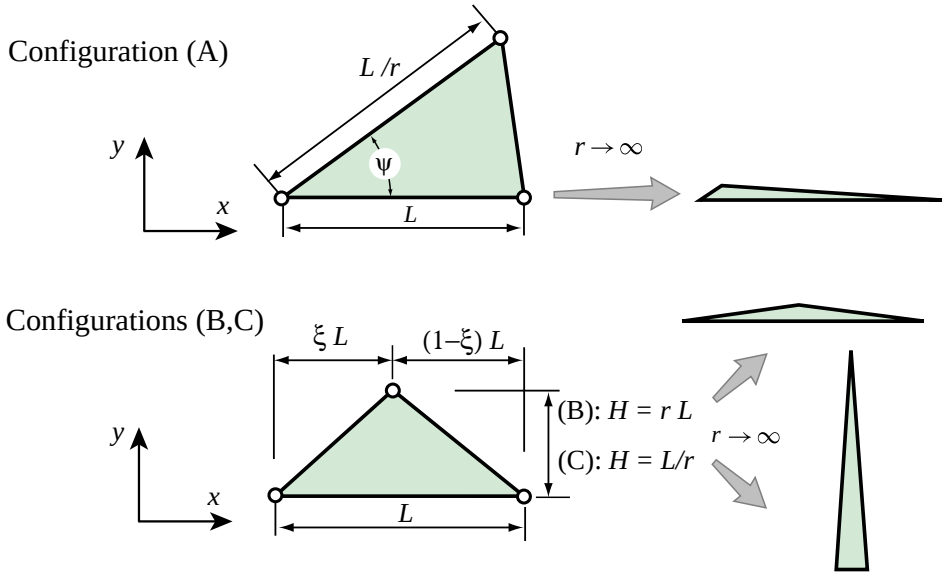

FIGURE 26.5. Triangle configurations for the study of ARI constraints.

from a general template such as KPT-1-36, to arrive at specific elements that display certain desirable characteristics. Experience shows that this is best done in two stages.

First, linear constraints on the free parameters are applied to generate *element families*. The dependence on the remaining free parameters is still linear.

Second, selected energy balance constraints are imposed. For linear elastic elements such constraints are quadratic in nature. Consequently there is no guarantee that real solutions exist. If they do, solutions typically produce families with few (usually 1 or 2) free parameters; in particular α families. Finally, setting the remaining parameters to specific values produces element instances.

§26.5. Linear Constraints

Three types of linear constraints have been used to generate element families.

§26.5.1. Observer Invariance (OI) Constraints

These pertain to *observer invariance*. If the element geometry exhibits symmetries, those must be reflected in the stiffness equations. For example, if the triangle becomes equilateral or isoceles, certain equality conditions between entries of the curvature-displacement matrices must hold. The resulting constraints are *linear* in the βs.

For the KPT-1-36 template one obtains the 14 constraints labeled as OI0 and OI1 in Table 26.3. The five OI0 constraints pertain to the order zero parameters and would be the only ones applicable to the KPT-1-9 template. They can be obtained by considering an equilateral triangle. The nine OI1 constraints link parameters of order one. This constraint set must be the first imposed and applies to any element.

§26.5.2. Aspect Ratio Insensitivity (ARI) Constraints

A second set of constraints can be found by requiring that the element be *aspect ratio insensitive*, or ARI for short, when subjected to arbitrary node displacements. A triangle that violates this requirement becomes infinitely stiff for certain geometries when a certain dimension aspect ratio r goes to infinite.

To express this mathematically, it is sufficient to consider the triangle configurations (A,B,C) depicted in Figure 26.5. In all cases L denotes a triangle dimension kept fixed while the aspect ratio r is increased. In configuration A, the angle ψ is kept fixed as $r \to \infty$. The opposite angles tend to zero and $\pi/2 - \psi$. The case $\psi = 90^\circ = \pi/2$ is particularly important as discussed later. In configurations (B) and (C) the ratio ξ is kept fixed as $r \to \infty$, and angles tend to π, $\pi/2$ or zero.

As higher order test displacements we select the four cubic modes $w_{30} = x^3$, $w_{21} = x^2y$, $w_{12} = xy^2$ and $w_{03} = y^3$. Any other cubic mode is a combination of those four. Construct the element energy ratios defined by Equation (26.5). The important dependence of those ratios on physical properties and free parameters is

$$\rho = \rho_b^m(r, \psi, \alpha) + \rho_h^m(r, \psi, \beta_j) \tag{26.9}$$

where $m = 30, 21, 12, 03$ identifies modes x^3, x^2y, xy^2 and y^3, respectively. (The dependence on L and constitutive matrix $\mathbf{D}$ is innocuous for this study and omitted for simplicity). Take a particular configuration (A,B,C) and mode m, and let $r \to \infty$. If ρ remains nonzero and bounded the element is said to be *aspect ratio insensitive* for that combination. If $\rho \to \infty$ the element is said to experience *aspect ratio locking*, whereas if $\rho \to 0$ the element becomes infinitely flexible. If ρ remains nonzero and bounded for all modes and configurations the element is called *completely aspect ratio insensitive*. The question is whether free parameters can be chosen to attain this goal.

As posed an answer appears difficult because the ratios (26.9) are quadratic in the free parameters, rational in r, and trascendental in ψ. Fortunately the question can be reduced to looking at the dependence of the *curvature-displacement* matrices on r as $r \to \infty$. Entries of these matrices are linear functions of the free parameters. As $r \to \infty$ no entry must grow faster than r, because exact curvatures grow as $O(r)$. For example, if an entry grows as r^2, setting its coefficient to zero provides a linear constraint from which the dependence on L and ψ is factored out. The material properties do not come in. Even with this substantial simplification the use of a CAS is mandatory to handle the elaborate symbolic algebra involved, which involves the Laurent expansion of all curvature matrices. The result of the investigation for the KPT-1-36 template can be summarized as follows.

(1) The basic energy ratio ρ_b is bounded for all ψ and all m in configuration (A). In configurations (B) and (C) it is unbounded as $O(r)$ in two cases: $m = 30$ if $\alpha \neq 1$, and $m = 21$ for any α.

(2) The higher order energy ratio ρ_h can be made bounded for all ψ and m by imposing the 18 linear constraints listed in Table 26.3 under the ARI label.

(3) The foregoing bound on ρ_h is not possible for the KPT-1-9 template. Thus a signature of the form (26.8) is undesirable from a ARI standpoint.

Because of the basic stiffness shortcoming noted in (1), a completely ARI element cannot be constructed. However, the βs can be selected to guarantee that ρ_h is always bounded. The resulting constraints are listed in Table 26.3. They are grouped in three subsets labeled ARI0, ARI1 and ARI2.

Subset ARI0 requires $\beta_{21} = \beta_{31} = \beta_{42} = \beta_{52} = \beta_{63} = \beta_{73} = 0$. If any of these 6 parameters is nonzero, one or more entries of the deviatoric curvature displacement matrices grow as r^3 in the 3 configurations. This represents disastrous aspect ratio locking and renders any such element useless.

Once OI0, OI1 and ARI0 are imposed, subset ARI1 groups 10 constraints obtained by setting to zero $O(r^2)$ grow in configuration (A) for all HO modes. This insures that $\rho = \rho_b + \rho_h$ stays bounded in that configuration (because ρ_b stays bounded for any α). In Table 26.3 they are listed in reverse order of that found by the symbolic analysis program, which means that the most important ones appear at the end.

Once OI0, OI1 and ARI0 and ARI1 are imposed, the 2-constraint subset ARI2 guarantees that ρ_h is bounded for configurations (B) and (C). Since ρ_b is not necessarily bounded in this case, these conditions

Table 26.4. Three Element Families Derivable From KPT-1-36

ARI(α,β_{10},β_{20},β_{30},γ_0,γ_1,γ_2)	α	β_{10}	β_{20}	β_{30}	β_{40}	$-\beta_{40}$	$-\beta_{30}$	$-\beta_{20}$	$-\beta_{10}$	0
		β_{11}	0	0	β_{41}	$-\beta_{61}$	β_{61}	β_{71}	$-\beta_{61}$	β_{61}
		β_{22}	β_{22}	β_{62}	0	0	β_{62}	β_{22}	β_{22}	β_{92}
		$-\beta_{61}$	β_{71}	β_{61}	$-\beta_{61}$	β_{41}	0	0	β_{11}	β_{61}
where $\beta_{40} = -\beta_{20} - \beta_{30} + \gamma_0$, $\beta_{11} = (2\beta_{10} + \beta_{20} + 3\beta_{30} - 4\beta_{40})/3 + \gamma_1$, $\beta_{22} = (8\beta_{20} - 4\beta_{30} + 2\beta_{40})/9 + \gamma_2$, $\beta_{61} = \beta_{20} - \beta_{22} - \beta_{30}$, $\beta_{41} = -\beta_{61} - 2\beta_{40}$, $\beta_{62} = \beta_{20} - \beta_{22} + \beta_{30}$, $\beta_{71} = -2\beta_{20} + \beta_{22}$ and $\beta_{92} = 2\beta_{10} - \beta_{11} + \beta_{20} + 3\beta_{30} - 4\beta_{40}$.										
ENO(α, β_{10}, β_{20}, β_{30}, β_{11}, β_{41}, β_{12}, β_{22}, β_{82}, β_{23}, β_{43}, β_{93})	α	β_{10}	β_{20}	β_{30}	β_{40}	$-\beta_{40}$	$-\beta_{30}$	$-\beta_{20}$	$-\beta_{10}$	0
		β_{11}	0	0	β_{41}	β_{43}	β_{33}	β_{23}	β_{81}	β_{93}
		β_{12}	β_{22}	β_{32}	0	0	β_{32}	β_{22}	β_{82}	β_{92}
		β_{13}	β_{23}	β_{33}	β_{43}	β_{41}	0	0	β_{83}	β_{93}
where $\beta_{40} = -\beta_{20} - \beta_{30}$, $\beta_{81} = -\beta_{12} + \beta_{93}$, $\beta_{32} = \beta_{23} + \beta_{41}$, $\beta_{92} = 2\beta_{11} - \beta_{12} + \beta_{82}$, $\beta_{13} = -\beta_{82} + \beta_{93}$, $\beta_{33} = \beta_{22} + \beta_{43}$ and $\beta_{83} = \beta_{11} - \beta_{12} + \beta_{82}$.										
ARIENO(α, β_{10}, β_{20}, β_{30})	ARI(α, β_{10}, β_{20}, β_{30}, 0, 0, 0)									

have minor practical importance.

Imposing OI0, OI1, ARI0 and ARI1 leaves $37 - 5 - 9 - 6 - 10 = 7$ free parameters, and produces the so-called ARI family defined in Table 26.4. Of the seven parameters, four are chosen to be the actual template parameters α, β_{10}, β_{20}, and β_{30}. Three auxiliary parameters, called γ_1, γ_2 and γ_3, are chosen to complete the generation of the ARI family as defined in Table 26.4.

This family is interesting in that it includes all existing high-performance elements, such as DKT and AQR1, as well as some new ones developed in the course of this study.

§26.5.3. Energy Orthogonality (ENO) Constraints

Energy orthogonality (ENO) means that the average value of deviatoric strains over the element is zero. Mathematically, $\mathbf{B}_{\chi 4} + \mathbf{B}_{\chi 5} + \mathbf{B}_{\chi 6} = \mathbf{0}$. This condition was a key part of the early developments of the Free Formulation by Bergan [12] and Bergan and Nygård [13], as well as of HP elements developed during the late 1980s and early 1990s.

The heuristic rationale behind ENO is to limit or preclude energy coupling between constant strain and higher order modes. A similar idea lurks behind the so-called "B-bar" formulation, which has a long and checkered history in modeling incompressibility and plastic flow.

For the KPT-1-36 element one may start with the OI0 and OI1 constraints as well as ARI0 (to preclude catastrophic locking), but ignoring ARI1 and ARI2. Then the ENO condition leads to the linear constraints labeled as ENO0 and ENO1 in Table 26.3. These group conditions on the order zero and one parameters, respectively. Imposing OI0, OI1, ARI0, ENO0 and ENO1 leads to the ENO family defined in Table 26.4, which has 12 free parameters. Elements ALR, FF0 and FF1 of Table 26.1 can be presented as instance of this family as shown later in a "genealogy" Table.

If instead one starts from the ARI family it can be verified that ENO is obtained if $\gamma_0 = \gamma_1 = \gamma_2 = 0$; that is, only three constraints are needed instead of five. [This is precisely the rationale for selecting those

"ENO deviations" as free arguments]. Moreover, the order-one constraints $\gamma_1 = \gamma_2 = 0$ are precisely ARI2 in disguise.

Setting $\gamma_0 = \gamma_1 = \gamma_2 = 0$ in ARI yields a four-parameter family called ARIENO (pronounced like the French "Arienne"). The free parameters are α, β_{10}, β_{20} and β_{30}. Its template is defined in Table 26.4. As noted, this family incorporates all constraints listed in Table 26.3. (These add up to 37 relations, but there are 4 redundancies.)

As noted all HP elements found to date are ARI (ALR, FF0 and FF1 are not considered HP elements now). Most are ENO, but there are some that are not. One example is HCTS, a "smoothed HCT" element developed in this study. Hence circumstantial evidence suggests that ARI is more important than ENO. In the present investigation ENO is used as a guiding principle rather than an *a priori* constraint.

§26.6. Quadratic Constraints

As noted in the foregoing section, the ARI family — and its ARIENO subset — is a promising source of high performance KPT elements. But seven parameters remain to be set to meet additional conditions. These fall into the general class of *energy balance* constraints introduced in [18]. Unit energy ratios are imposed for specific mesh unit geometries, loadings and boundary conditions. Common feature of such constraints, for linear elements, are: they involve constitutive properties, and they are *quadratic* in the free parameters. Consequently real parameter solutions are not guaranteed. Even if they have real solutions, the resulting families may exist only for limited parameter ranges.

Numerous variants of the energy balance tests have been developed over the years. Because of space constraints only three variations under study are described below. All of them have immediate physical interpretation in terms of the design of custom elements. They have been applied assuming isotropic material with zero Poisson's ratio.

§26.6.1. Morphing Constraints

This is a class of constraints that is presently being studied to ascertain whether enforcement would be generally beneficial to element performance. Consider the two-KPT-element rectangular mesh unit shown in Figure 26.6. The aspect ratio r is the ratio of the longest rectangle dimension L to the width $b = L/r$. The plate is fabricated of a homogeneous isotropic material with zero Poisson's ratio and thickness t. Axis x is selected along the longitudinal direction. We study the two *morphing processes* depicted at the top of Figure 26.6. In both the aspect ratio r is made to increase, but with different objectives.

Plane Beam Limit. The width $b = L/r$ is decreased while keeping L and t fixed. The limit is the thin, Bernoulli-Euler plane beam member of rectangular cross section $t \times b$, $b << t$, shown at the end of the beam-morphing arrow in Figure 26.6. This member can carry exactly a linearly-varying bending moment $M(x)$ and a constant transverse shear V, although shear deformations are not considered.

Twib Limit. Again the width $b = L/r$ is decreased by making r grow. The thickness t, however, is still considered small with respect to b. The limit is the twisted-ribbon member of cross section $t \times b$, $t << b$, shown on the left of Figure 26.6. This member, called a "twib" for brevity, can carry a longitudinal torque $T(x)$ that varies linearly in x.

Conditions called *morphing constraints* are now posed as follows.

(1) Does the mesh unit approach the exact behavior of a Hermitian cubic beam as $r \to \infty$? If so, the plate element is said to be *beam morphing exact* or BE for short.

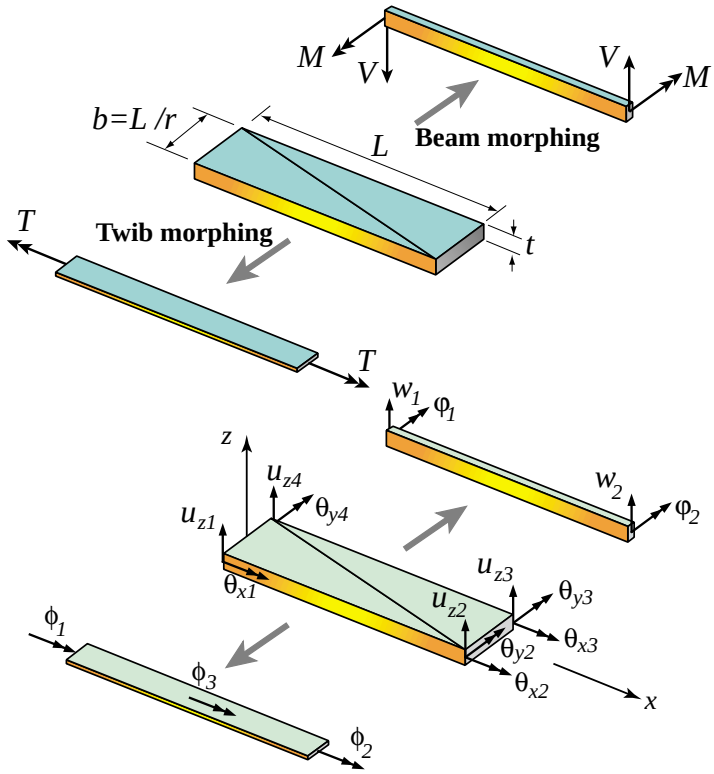

FIGURE 26.6. Morphing a rectangular plate mesh unit to beam and twib.

(2) Does the mesh unit approach the exact beam behavior as both $r \to \infty$ and $r \to 0$? If so, the plate element is said to be *double beam morphing exact* or DBE for short.

(3) Does the mesh unit approach the exact behavior of a twib under linearly varying torque? If so, the plate element is said to be *twib-morphing-exact* or TE.

To check these conditions the 12 plate-mesh-unit freedoms are congruentially transformed to the beam and twib freedoms shown at the bottom of Figure 26.6. The BE and TE conditions can be derived by symbolically expanding these transformed stiffness equations in Laurent series as $r \to \infty$. The DBE condition requires also a Taylor expansion as $r \to 0$. They can also be derived as asymptotic forms of energy ratios.

An element satisfying (1) and (3) is called BTE, and one satisfying (1), (2) and (3) is called DBTE. The practical interest for morphing conditions is the appearance of very high aspect ratios in modeling certain aerospace structures, such as the stiffened panel depicted in Figure 26.7.

§26.6.2. Mesh Direction Insensitivity Constraints

This class of constraints is important in high frequency and wave propagation dynamics to minimize mesh induced anisotropy and dispersion. One important application of this kind of analysis is simulation of nondestructive testing of microelectronic devices and thin films by acoustic imaging.

Consider a square mesh unit fabricated of 4 overlapped triangles to try to minimize directionality from the start. Place Cartesian axes x and y at the mesh unit center. Apply higher order modes x_φ^3 and $x_\varphi^2 y_\varphi$, where x_φ forms an angle φ from x, and require that $\rho = 1$ for all φ. Starting from ARIENO one can construct α families which satisfy that constraint. The simplest one is the MDIT(α) family, which for $\alpha = 1$ yields the element MDIT1 defined in Table 26.5.

Table 26.5. Template Signatures of Selected New KPT Elements

Acronym	α	β_{1j}	β_{2j}	β_{3j}	β_{4j}	β_{5j}	β_{6j}	β_{7j}	β_{8j}	β_{9j}	β_{sc}
BTE13	1/3	−9	2	−1	−1	1	1	−2	9	0	/6
		−5	0	0	1	−1	1	−2	−1	1	
		2	2	−1	0	0	−1	2	2	−10	
		−1	−2	1	−1	1	0	0	−5	1	
DBE00	ARIENO(0, $-3/2$, β_{20}, β_{30}), with $\beta_{20} = 3\left(\sqrt{6}-2\right)/4$ and $\beta_{30} = -\beta_{20}$.										
DBE13	ARIENO(1/3, $-3/2$, β_{20}, β_{30}) with $\beta_{20} = -3/2 - \left(\sqrt{25-\sqrt{609}}\right)/12 + \left(25+\sqrt{609}\right)/4$ and $\beta_{30} = 3/2 - \left(\sqrt{25-\sqrt{609}}\right)/12 - \left(25+\sqrt{609}\right)/4$.										
DBE12	ARIENO(1/2, $-3/2$, β_{20}, β_{30}) with $\beta_{20} = \left(-12-\sqrt{10-2\sqrt{21}}+3\sqrt{10+2\sqrt{21}}\right)/8$ and $\beta_{30} = \left(12-\sqrt{10-2\sqrt{21}}-3\sqrt{10+2\sqrt{21}}\right)/8$.										
DBEN00	0	−3	0	0	0	0	0	0	3	0	/2
		2	0	0	0	0	0	0	0	0	
		0	0	0	0	0	0	0	0	−8	
		0	0	0	0	0	0	0	2	0	
DBEN13	1/3	−27	−1	−1	2	−2	1	1	27	0	/18
		$4\sqrt{61}-22$	0	0	−4	0	0	2	0	0	
		0	0	−2	0	0	−2	0	0	$-4(\sqrt{61}+11)$	
		0	2	0	0	−4	0	0	$4\sqrt{61}-22$	0	
DBEN12	1/2	−12	−1	−1	2	−2	1	1	12	0	/8
		$4(\sqrt{6}-3)$	0	0	−4	0	0	2	0	0	
		0	0	−2	0	0	−2	0	0	$-4(\sqrt{6}+6)$	
		0	2	0	0	−4	0	0	$4(\sqrt{6}-3)$	0	
DBTE13	ARIENO(1/3, −1.3100926, 0.40467862, −0.49926464)										
HCTS	1	−18	5	5	−1	1	−5	−5	18	0	/12
		8	0	0	2	0	0	−10	0	0	
		0	0	10	0	0	10	0	0	−20	
		0	−10	0	0	2	0	0	8	0	
MDIT1	1	−45	6	−6	0	0	6	−6	45	0	/30
		−34	0	0	−4	−4	4	−4	−4	4	
		8	8	−8	0	0	−8	8	8	−68	
		−4	−4	4	−4	−4	0	0	−34	4	

The correlation of this condition to flexural wave propagation and its extension to more general element lattices is under study.

§26.6.3. Distortion Minimization Constraints

An element is distortion insensitive when the solution hardly changes even when the mesh is significantly changed. The precise quantification of this definition in terms of energy ratios on standard benchmarks tests is presently under study. Preliminary conclusions suggest that sensitivity to distortion is primarily controlled by the basic stiffness parameter α whereas the higher order parameters βs only play a secondary role. For the KPT-1-36 template, $\alpha = 1$ appears to minimize the distortion sensitivity in ARIENO elements.

Table 26.6. Brief Description of New Elements Listed in Table 26.5

Name	Description
BTE13	Instance of the BTE(α) family for $\alpha = 1/3$. This is a subset of ARIENO which exhibits beam morphing and twib morphing exactness in the sense discussed in Section 6.1.
DBE00,DBE13, DBE12	Instances of the DBE(α) family for $\alpha = 0$, $\alpha = 1/3$ and $\alpha = 1/2$, respectively. DBE(α) is a subset of ARIENO which exhibits double-beam morphing exactness. The family exists (in the sense of having real solutions) for $\alpha \leq 1/\sqrt{2}$.
DBEN00,DBEN13, DBEN12	Instances of the DBEN(α) family for $\alpha = 0$, $\alpha = 1/3$ and $\alpha = 1/2$, respectively. Family exhibits double-beam morphing exactness but is not ENO. Exists for $\alpha \leq 1/\sqrt{2}$. DBEN00 coalesces with ALR.
DBTE13	An ARIENO instance with $\alpha = 1/3$ which exhibits double-beam and twib morphing exactness. It was found by minimizing a residual function. Only numerical values for the parameters are known. Such elements seem to exist only for a small α range.
HCTS	Derived from HCT, which is a too-stiff poor performer, by smoothing its curvature field. It displays very high performance if beam or twib exactness is not an issue. Member of ARI but not ARIENO.
MDIT1	Instance of the MDIT(α) family for $\alpha = 1$. MDI stands for Mesh-Direction Insensitive. Such elements display stiffness isotropy when assembled in a square mesh unit. Primarily of interest in high frequency dynamics as discussed in Section 7.2. Static performance also good to excellent for rectangular mesh units.

Table 26.7. Genealogy of Specific KPT Elements

Name	Source Family
ALR	ARI(0, $-3/2$, 0, 0, 0, -2, 0)
AQR1	ARIENO(1, $-3/2$, 0, 0)
AQR0	ARIENO(0, $-3/2$, 0, 0)
AQRBE	ARIENO($1/\sqrt{2}$, $-3/2$, 0, 0)
AVG	ENO(0, $-3/2$, 0, 0, 0, 0, 0, 0, 0, 0, 0, 0)
BCIZ0 (and clones), BCIZ1, HCT	Not ARI or ENO
BTE13	ARIENO(1/3, $-3/2$, 1/3, $-1/6$)
DBE00, DBE13, DBE12	See Table 26.5
DBEN00	ARI(0, $-3/2$, 0, 0, 0, 2, 0)
DBEN13	ARI(0, $-3/2$, $-1/18$, $-1/18$, 0, $2\sqrt{61}/9$, 0)
DBEN12	ARI(0, $-3/2$, $-1/8$, $-1/8$, 0, $\sqrt{3/2}$, 0)
DKT	ARIENO(1, $-3/2$, 1/4, 1/4)
FF0 (and clones)	ENO(0, $-3/2$, 1/6, 1/6, 0, 0, 0, 0, 0, 0, 0, 0)
FF1	ENO(1, $-3/2$, 1/6, 1/6, 0, 0, 0, 0, 0, 0, 0, 0)
HCTS	ARI(1, $-3/2$, 5/12, 5/12, 3/4, 1, $-1/6$)
MDIT1	ARIENO(1, $-3/2$, 1/5, $-1/5$)

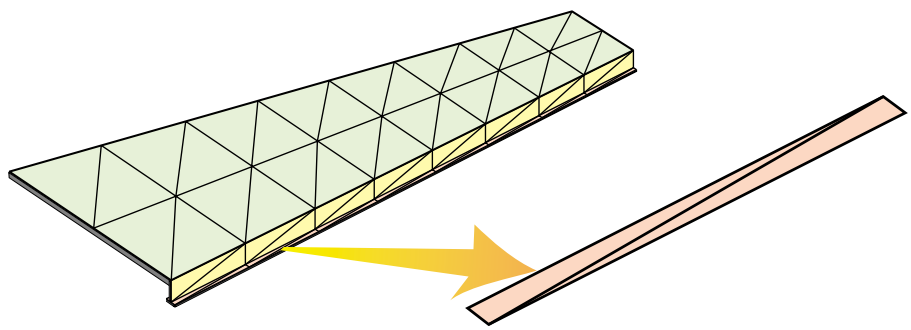

FIGURE 26.7. Stiffened panels modeled by facet shell elements are a common source of high aspect ratio elements.

§26.7. New KPT Elements

Starting from the ARI family and applying various energy constraints, a set of new elements with various custom properties have been developed in this study. The most promising ones are listed in Tables 26.5 and chapdot6. Table 26.7 gives the genealogy — in the sense of "element family membership" — of all elements listed in Tables 26.1 and 26.6.

The performance of the old and new elements in a comprehensive set of plate bending benchmarks is still in progress. Preliminary results are reported in the next Section. It should be noted that the unification brought about by the template approach is facilitated for such comparisons, because all possible elements of a given type and node/freedom configuration can be implemented with a single program module. Furthermore the error-prone process of codifying somebody else's published element is reduced as long as the signature is known.

§26.8. Benchmark Studies

Only a limited number of benchmark studies have been conducted to compare the new BTME elements with existing ones. One unfinished ingredient is the formulation of consistent node forces for distributed loads. These are difficult to construct because no transverse displacement shape functions are generally available, and the topic (as well as the formulation of consistent mass and geometric stiffness) will require further research. In all tests reported below the material is assumed isotropic with zero Poisson's ratio.

§26.8.1. Simply Supported and Clamped Square Plates

The first test series involved the classical problem of a square plate with simply supported and clamped boundary conditions, subjected to either a uniform distributed load, or a concentrated central load. Only results for the latter are shown here. Meshes of $N \times N$ elements over one quadrant were used, with $N = 1, 2, 4, 8$ and 16. Mesh units are formed with four overlapped half-thickness elements to eliminate diagonal directionality effects.

The accuracy of the computed central deflection w_C is reported as $d = -\log_{10} \epsilon_{rel}$ where ϵ_{rel} is the relative error $\epsilon_{rel} = |(w_C - w_{Cex})/w_{Cex}|$, w_{Cex} being the exact value that is known to at least five places; see [19]. Using d has the advantage of giving at a glance the number of correct digits. A shortcoming of d is that it ignores deflection error signs; this occasionally induces spurious "accuracy spikes" if computed results cross over the exact value before coming back. For this load case d also measures the energy accuracy.

Figure 26.8 displays log-log error plots in which d is shown as a function of $\log_2 N$. The ultimate slope of the log-log curve characterizes the asymptotic energy convergence rate. The plots indicate an asymptotic

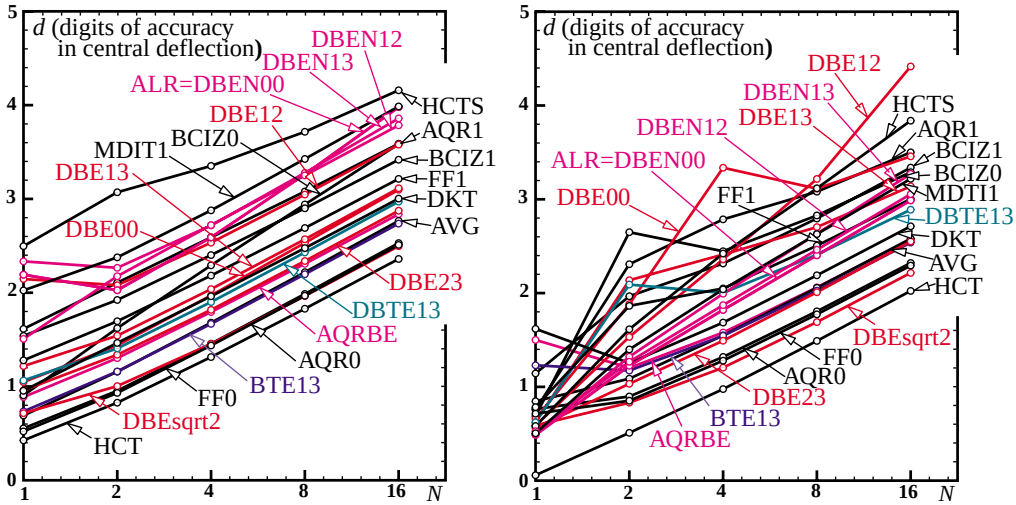

FIGURE 26.8. Convergence study of SS and clamped square plates under concentrated central load.

rate of $O(1/N^2)$ for all elements, meaning that ultimately a doubling of N gives $\log_{10} 4 \approx 0.6$ more digits. The same $O(h^2)$ convergence rate was obtained for energy, displacements, centroidal curvatures and centroidal moments, although only displacements are reported here.

Although the asymptotic convergence rate is the same for all elements in the template, big differences as regards error coefficients can be observed. These differences are visually dampened by the log scale. In both problems the difference between the worst element (HCT) and the best ones (HCTS, MDIT1, AQR1) spans roughly two orders of magnitude. The performance of the new BE and DBE elements depends significantly on the α parameter, with DBEN12, DBEN13 and DBE12 generally outperforming the others. The sanitized BCZ elements do well. DKT, FF0 and FF1 come in the middle of the pack. The results for distributed loads, not reported here, as well 2:1 rectangular plates largely corroborate these rankings, except for deteriorating performance of the BCZ elements.

§26.8.2. Uniformly Loaded Cantilever

Figure 26.9 reports the convergence study of a narrow cantilever plate subjected to uniform lateral load q. The aspect ratio is $r = 20$. Regular $N \times N$ meshes are used, with $N = 1, 2, 4$ and 8. The consistent transformation of q to node forces has not been investigated. The analysis uses the consistent loads of FF0, for which the transverse displacement over the triangle is available. This shortcut is not believed to have a major effect on convergence once the mesh is sufficiently fine.

As expected the beam-exact elements do much better than the others, with an accuracy advantage of 3-4 orders of magnitude for $N \geq 4$. (The different superconvergence slopes have not been explained yet in term of asymptotic expansions, pending a study of consistent load formulations.) The accuracy "spike" of DBE13 is a fluke caused by computed end deflections crossing over the exact answer before returning to it.

§26.8.3. Aspect Ratio Test of End Loaded Cantilever

Aspect ratio tests use a single mesh unit of length L and width $b = L/r$ subjected to simple end load systems. Only r is varied. Two kinds of tests, depicted in Figures 26.10 and 26.11, were carried out.

The analysis of the shear-end-loaded cantilever mesh unit, reported in Figure 26.10, simply confirms the asymptotic analysis of the beam morphing process. As expected, the BE and DBE elements designed

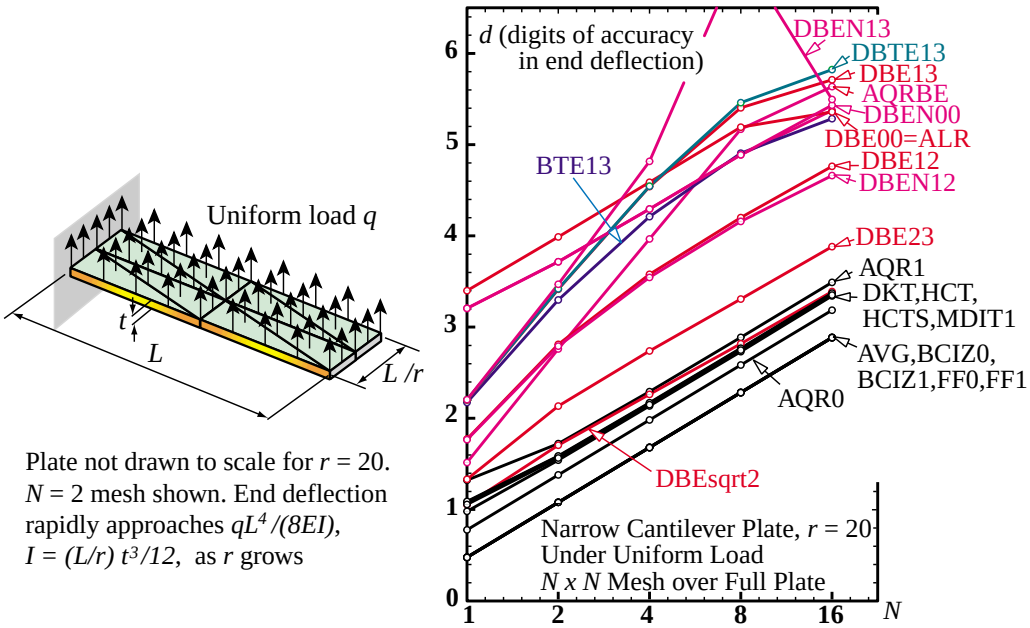

FIGURE 26.9. Convergence study of uniform loaded, narrow cantilever plate.

to beam-morph exactly perform well, converging to the correct thin-cantilever answer $PL^3/(3EI)$ as $r \to \infty$. All other elements stay at the same deflection percentage beyond $r > 8$. For example, the five elements AVG, BCIZ0, BCIZ1, FF0 and FF1 yield 2/3 of the correct answer whereas DKT, MDIT1 yields 3/4 of it.

The end load system must include two fixed-end moments $\pm\alpha PLr/12$ to deliver the correct answers predicted by the $r \to \infty$ asymptotic analysis. Should the moments be removed, significant errors occur if $\alpha \neq 0$, and BME mesh units no longer converge to the correct answer as $r \to \infty$. Of course, in the case of a repeated mesh subdivision the effect of those moments would become progressively smaller.

§26.8.4. Aspect Ratio Test of Twisted Ribbon

Aspect ratio tests were also conducted on a twib subjected to a total applied end torque T using a single mesh unit fabricated of 4 overlaid triangles to avoid directional anisotropy. The consistent nodal force system shown in Figure 26.11 was used. Two boundary condition cases: (I) and (II), also defined in Figure 26.11, were considered.

Case (I) is essentially a constant twist-moment patch test. All elements in the KPT-1-36 template must pass the test, and indeed all elements gave the correct answer for any r. The total angle of twist must be $\phi_E = TL/GJ$, where $G = \frac{1}{2}E$ (because $\nu = 0$) and $J = \frac{1}{3}(L/r)t^3$. With the boundary conditions set as shown, the x rotations at both end nodes must be ϕ_E, the transverse deflections $\pm\phi_E(L/2r)$ and the y rotations $\pm\phi_E/(2r)$. Note, however, that if the applied load system shown in Figure 26.11 is not adhered to, the patch test is not passed. For example, the end moments cannot be left out unless $\alpha = 1$. This consistency result is believed to be new.

Case (II) is analogous to Robinson's twisted ribbon test [34], which is usually conducted with specific material and geometric properties. Working with symbolic algebraic computations there is no need to chose arbitrary numerical values. The end torque T was simply adjusted so that the pure twist solution gives $\phi_E = r$. The graph shown on the right of Figure 26.11 plots ϕ_E as function of r for specific

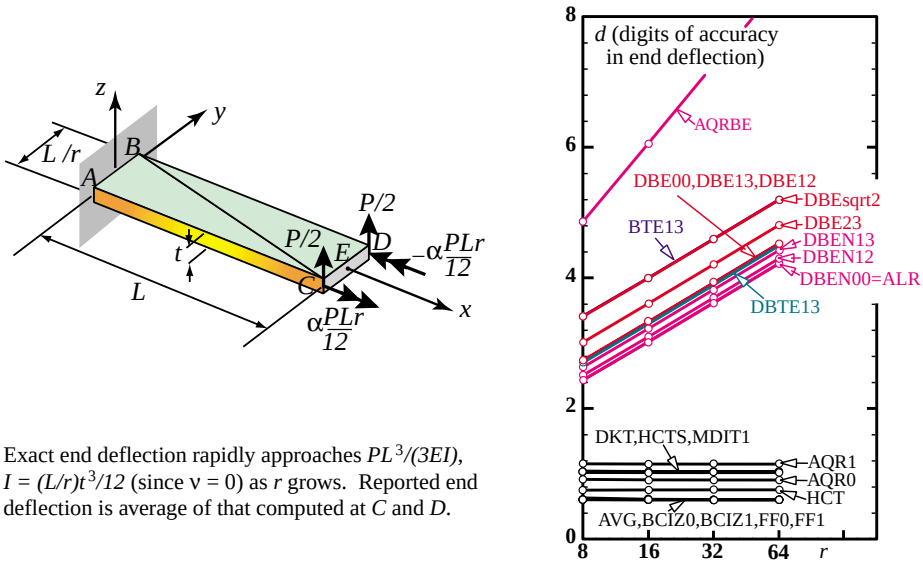

FIGURE 26.10. Aspect ratio study of end-loaded cantilever mesh unit.

elements in the range $r = 5$ to $r = 40$. Because the sign of the discrepancy is important, this plot does not use a log-log reduction. It is seen that most elements are too stiff, and that several of them, notably HCT, BCIZ and FF, exhibit severe aspect ratio locking. For the twib-exact (TE) elements, a symbolic analysis predicted that exact agreement with the pure twist solution for this boundary condition case can only be obtained if $\alpha = 1/3$. The computed response of BTE13 and DBTE13 verifies this prediction.

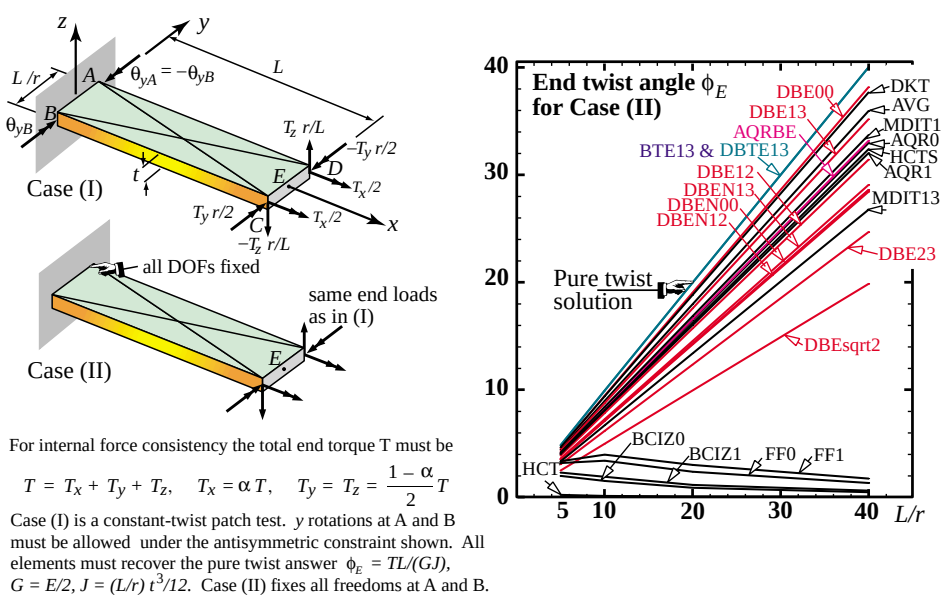

FIGURE 26.11. Twisted ribbon test.

§26.8.5. The Score so Far

The benchmarks conducted so far, of which those reported in Section 8 constitute a small sample, suggest that the choice of an optimal "element for all seasons" will not be realized. For the classical rectangular

plate benchmarks HCTS, MDTI1 and AQR1 consistently came at the top. The displacement-assumed HCT, BCZ and FF elements, which represent 1970-80 technology, did well for unit aspect ratios but deteriorated for narrower triangles. The new BE and DBE elements showed variable performance. The performance of DKT was mediocre to average. Skew plate tests, not reported here, were inconclusive.

For problems typified by uniaxial bending of long cantilevers, the BE and DBE elements outperformed all others as can be expected by construction. The displacement assumed elements did poorly. Distortion benchmarks, not reported here, indicate that ARI elements with $\alpha = 1$ outperform elements with $\alpha \neq 1$, or non-ARI elements such as FF1 or HCT.

Based on the test set, MDIT1 and HCTS appear to the running neck and neck as the best all-purpose KPT elements, closely followed by AQR1. There are arguments for DBE13 as good choice for very high aspect ratio situations such as the stiffened panels illustrated in Figure 26.7. Unfortunately directly joining elements with different αs would violate the IET. Thus a mesh with, say, DBE13 in high aspect ratio regions and HCTS otherwise would be disallowed. Such combinations could be legalized by interface transition elements but that would represent a new research topic.

§26.9. Concluding Remarks

The usual finite element construction process, which involves *a priori* selection of a variational principle and shape functions, hinders the exploration of a wide range of admissible finite element models. As such it is ineffectual for the *design* of finite elements with desirable physical behavior. The application described here illustrates the effectiveness of templates to build custom elements. The template approach attempts to implement the hope long ago expressed by Bergan and Hanssen [24] in the Introduction of their MAFELAP II paper:

> "An important observation is that each element is, in fact, only represented by the numbers in its stiffness matrix during the analysis of the assembled system. The origin of these stiffness coefficients is unimportant to this part of the solution process ... The present approach is in a sense the opposite of that normally used in that the starting point is a generally formulated convergence condition and from there the stiffness matrix is derived ... The patch test is particularly attractive [as such a condition] for the present investigation in that it is a direct test on the element stiffness matrix and requires no prior knowledge of interpolation functions, variational principles, etc."

This statement sets out what may be called the *direct algebraic approach* to finite elements: the element stiffness is derived directly from consistency conditions — provided by the IET — plus stability and accuracy considerations to determine algebraic redundancies if any. It has in fact many points in common with energy-based finite differences.

This ambitious goal has proven elusive because the direct algebraic construction of the stiffness matrix of most multidimensional elements becomes effectively a problem in constrained optimization. In the *symbolic form* necessitated by element design, such problem is much harder to tackle than the conventional element construction methods based on shape functions. Only with the advent and general availability of powerful computer algebra systems can the dream become a reality.

Acknowledgements

Preparation of the present paper has been supported by the National Science Foundation under Grant ECS-9725504, and by Sandia National Laboratories under the Advanced Strategic Computational Initiative (ASCI) Contract BF-3574.

References

[1] Turner, M. J., Clough, R. W., Martin, H. C., Topp, L. J., "Stiffness and Deflection Analysis of Complex Structures," *J. Aero. Sci.*, **23**, 805–824, 1956.

[2] Clough, R. W., "The Finite Element Method in Plane Stress Analysis," *Proc. 2nd ASCE Conference on Electronic Computation*, Pittsburgh, PA, 1960.

[3] Zienkiewicz, O. C., Cheung, Y. K., *The Finite Element Method in Engineering Science*, McGraw-Hill, New York, 1967.

[4] Strang, G., Fix, G., *An Analysis of the Finite Element Method*. Prentice-Hall, 1973.

[5] Courant, R., "Variational Methods for the Solution of Problems in Equilibrium and Vibrations," *Bull. Amer. Math. Soc.*, **49**, 1–23, 1943; reprinted in *Int. J. Numer. Meth. Engrg.*, **37**, pp. 643ff, 1994.

[6] Argyris, J. H., Kelsey, S., *Energy Theorems and Structural Analysis*. London, Butterworth, 1960; Part I reprinted from *Aircr. Engrg.* **26**, Oct-Nov 1954 and **27**, April-May 1955.

[7] Turner, M. J., "The Direct Stiffness Method of Structural Analysis, Structural and Materials Panel Paper," AGARD Meeting, Aachen, Germany, 1959.

[8] Turner, M. J., Martin, H. C., Weikel, R. C., "Further Development and Applications of the Stiffness Method," in *AGARDograph 72: Matrix Methods of Structural Analysis*, ed. by B. M. Fraeijs de Veubeke, Pergamon Press, New York, 203–266, 1964.

[9] Felippa, C. A., "Parametrized Unification of Matrix Structural Analysis: Classical Formulation and d-Connected Mixed Elements," *Finite Elem. Anal. Des.*, **21**, 45–74, 1995.

[10] Felippa, C. A., Militello, C., "Developments in Variational Methods for High Performance Plate and Shell Elements," in *Analytical and Computational Models for Shells*, CED Vol. 3, ed. by A. K. Noor, T. Belytschko and J. C. Simo, ASME, New York, 191–216, 1989.

[11] Zienkiewicz, O. C., Taylor, R. E., *The Finite Element Method*, Vol. I, 4th ed. McGraw-Hill, New York, 1989.

[12] Bergan, P. G., "Finite Elements Based on Energy Orthogonal Functions," *Int. J. Numer. Meth. Engrg.*, **15**, 1141–1555, 1980.

[13] Bergan, P. G., Nygård, M. K., "Finite Elements with Increased Freedom in Choosing Shape Functions," *Int. J. Numer. Meth. Engrg.*, **20**, 643–664, 1984.

[14] MacNeal, R. H., "Derivation of Element Stiffness Matrices by Assumed Strain Distribution," *Nuclear Engrg. Design*, **70**, 3–12, 1978.

[15] Bathe, K. J., Dvorkin, E. N., "A Four-Node Plate Bending Element Based on Mindlin-Reissner Plate Theory and a Mixed Interpolation," *Int. J. Numer. Meth. Engrg.*, **21**, 367–383, 1985.

[16] Park, K. C., Stanley, G. M., "A Curved C^0 Shell Element Based on Assumed Natural-Coordinate Strains," *J. Appl. Mech.*, **53**, 278–290, 1986.

[17] Simo, J. C., Hughes, T. J. R., "On the Variational Foundations of Assumed Strain Methods," *J. Appl. Mech.*, **53**, 51–54, 1986.

[18] Bergan, P. G., Felippa, C. A., "A Triangular Membrane Element with Rotational Degrees of Freedom," *Comp. Meths. Appl. Mech. Engrg.*, **50**, 25–69, 1985.

[19] Felippa, C. A., Bergan, P. G., "A Triangular Plate Bending Element Based on an Energy-Orthogonal Free Formulation," *Comp. Meths. Appl. Mech. Engrg.*. **61**, 129–160, 1987.

[20] Militello, C., Felippa, C. A., "The First ANDES Elements: 9-DOF Plate Bending Triangles," *Comp. Meths. Appl. Mech. Engrg.*, **93**, 217–246, 1991.

[21] Felippa, C. A., Militello, C., "Membrane Triangles with Corner Drilling Freedoms: II. The ANDES Element," *Finite Elem. Anal. Des.*, **12**, 189–201, 1992.

[22] Felippa, C. A., "A Survey of Parametrized Variational Principles and Applications to Computational Mechanics," *Comp. Meths. Appl. Mech. Engrg.*, **113**, 109–139, 1994.

[23] Felippa, C. A., "Recent Developments in Parametrized Variational Principles for Mechanics," *Comput. Mech.*, **18**, 159–174, 1996.

[24] Bergan, P. G., Hanssen, L., "A New Approach for Deriving 'Good' Finite Elements," in *The Mathematics of Finite Elements and Applications – Volume II*, ed. by J. R. Whiteman, Academic Press, London, 483–497, 1975.

[25] Felippa, C. A., Haugen, B., Militello, C., "From the Individual Element Test to Finite Element Templates: Evolution of the Patch Test," *Int. J. Numer. Meth. Engrg.*, **38**, 199–222, 1995.

[26] Bazeley, G. P., Cheung, Y. K., Irons, B. M., Zienkiewicz, O. C., "Triangular Elements in Plate Bending —

Conforming and Nonconforming Solutions," in *Proc. 1st Conf. on Matrix Methods in Structural Mechanics*, AFFDL-TR-66-80, Air Force Institute of Technology, Dayton, Ohio, 547–584, 1966.

[27] Hanssen, L., Bergan, P. G., Syversten, T. J., "Stiffness Derivation Based on Element Convergence Requirements" in *The Mathematics of Finite Elements and Applications – Volume III*, ed. by J. R. Whiteman, Academic Press, London, 83–96, 1979.

[28] Argyris, J., Tenek, L., Olofsson, L., "TRIC: a Simple but Sophisticated 3-node Triangular Element based on 6 Rigid Body and 12 Straining Modes for Fast Computational Simulations of Arbitrary Isotropic and Laminate Composite Shells," *Comp. Meths. Appl. Mech. Engrg.*, **145**, 11–85, 1997.

[29] Nygård, M. K., "The Free Formulation for Nonlinear Finite Elements with Applications to Shells," Ph. D. Dissertation, Division of Structural Mechanics, NTH, Trondheim, Norway, 1986.

[30] Stricklin, J., Haisler, W., Tisdale, P., Gunderson, R., "A Rapidly Converging Triangular Plate Bending Element," *AIAA J.*, **7**, 180–181, 1969.

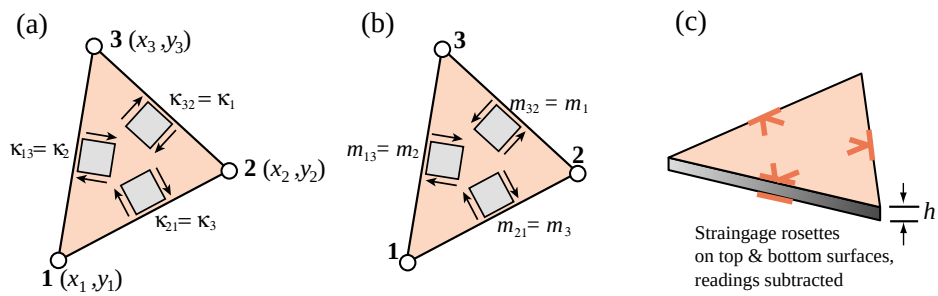

FIGURE 26.12. Natural curvatures and bending moments.

[31] Batoz, J. L. "An Explicit Formulation for an Efficient Triangular Plate-Bending Element," *Int. J. Numer. Meth. Engrg.*. 18:1077–1089, 1982.

[32] Batoz, J. L., Bathe K.-J., Ho, L. W., "A Study of Three-Node Triangular Plate Bending Elements," *Int. J. Numer. Meth. Engrg.*, **15**, 1771–1812, 1980.

[33] Clough, R. W., Tocher, J. L., "Finite Element Stiffness Matrices for the Analysis of Plate Bending," in *Proc. 1st Conf. on Matrix Methods in Structural Mechanics*, AFFDL-TR-66-80, Air Force Institute of Technology, Dayton, Ohio, 515–547, 1966.

[34] Robinson, J., Haggenmacher, G. W., "LORA – An Accurate Four-Node Stress Plate Bending Element," *Int. J. Numer. Meth. Engrg.*, **14**, 296–306, 1979.

Appendix 26.A. Formulation of KPT-1-36 Template

This Appendix collects the formulas that fully define the KPT-1-36 element template.

§26.A.1. Element Relations

The triangle geometry is defined by the corner coordinates in its (x, y) local system, which are (x_i, y_i), $i = 1, 2, 3$. Coordinate differences are abbreviated as $x_{ij} = x_i - x_j$ and $y_{ij} = y_i - y_j$. The signed triangle area A is given by $2A = x_{21}y_{31} - x_{31}y_{21} = x_{32}y_{12} - x_{12}y_{32} = x_{13}y_{23} - x_{23}y_{13}$ and we require that $A > 0$. The visible degrees of freedom of the element collected in $\mathbf{u}$ and the associated node forces collected in $\mathbf{f}$ are

$$\mathbf{u}^T = [\, u_{z1} \quad \theta_{x1} \quad \theta_{y1} \quad u_{z2} \quad \theta_{x2} \quad \theta_{y2} \quad u_{z3} \quad \theta_{x3} \quad \theta_{y3} \,]. \tag{26.10}$$

$$\mathbf{f}^T = [\, f_{z1} \quad \mathcal{M}_{x1} \quad \mathcal{M}_{y1} \quad f_{z2} \quad \mathcal{M}_{x2} \quad \mathcal{M}_{y2} \quad f_{z3} \quad \mathcal{M}_{x3} \quad \mathcal{M}_{y3} \,]. \tag{26.11}$$

The Cartesian components of the plate curvatures are κ_{xx}, κ_{yy} and $2\kappa_{xy} = \kappa_{xy} + \kappa_{yx}$, which are gathered in a 3-vector $\boldsymbol{\kappa}$. In the Kirchhoff model, curvatures and displacements are linked by

$$\kappa_{xx} = \frac{\partial^2 w}{\partial x^2}, \qquad \kappa_{yy} = \frac{\partial^2 w}{\partial y^2}, \qquad 2\kappa_{xy} = 2\frac{\partial^2 w}{\partial x \partial y}. \tag{26.12}$$

where $w = w(x, y) \equiv u_z$ is the plate transverse displacement. In the KPT elements considered here, however, the compatibility equations (26.12) must be understood in a weak sense because the assumed curvature field is not usually integrable. The internal moment field is defined by the Cartesian components m_{xx}, m_{yy} and m_{xy}, which are placed in a 3-vector $\mathbf{m}$. Curvatures and moments are linked by the constitutive relation

$$\mathbf{m} = \begin{bmatrix} m_{xx} \\ m_{yy} \\ m_{xy} \end{bmatrix} = \begin{bmatrix} D_{11} & D_{12} & D_{13} \\ D_{12} & D_{22} & D_{23} \\ D_{13} & D_{23} & D_{33} \end{bmatrix} \begin{bmatrix} \kappa_{xx} \\ \kappa_{yy} \\ 2\kappa_{xy} \end{bmatrix} = \mathbf{D}\boldsymbol{\kappa}. \tag{26.13}$$

where $\mathbf{D}$ results from integration through the thickness in the usual way. Three dimensionless side direction coordinates π_{21}, π_{32} are π_{13} are defined as going from 0 to 1 by marching along sides 12, 23 and 31, respectively.

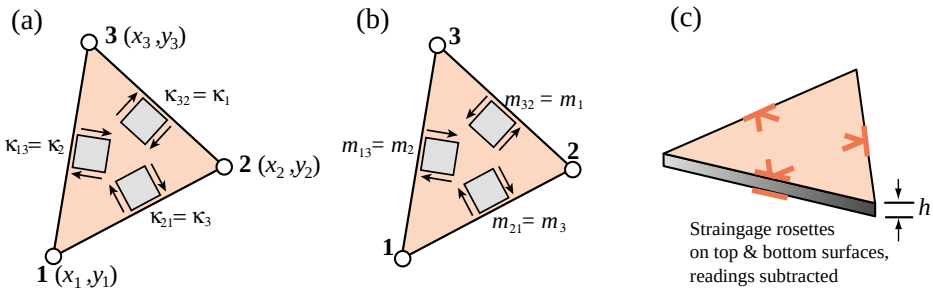

FIGURE 26.13. Natural curvatures and bending moments.

The side coordinate π_{ji} of a point not on a side is that of its projection on side ij. The second derivatives of $w \equiv u_z$ with respect to the dimensionless side directions will be called the *natural curvatures* and are denoted by $\chi_{ji} = \partial^2 w/\partial\pi_{ji}^2$. These curvatures have dimensions of displacement. They are related to the Cartesian plate curvatures by the matrix relation

$$\boldsymbol{\chi} = \begin{bmatrix} \chi_{21} \\ \chi_{32} \\ \chi_{13} \end{bmatrix} = \begin{bmatrix} \dfrac{\partial^2 w}{\partial \pi_{21}^2} \\ \dfrac{\partial^2 w}{\partial \pi_{32}^2} \\ \dfrac{\partial^2 w}{\partial \pi_{13}^2} \end{bmatrix} = \begin{bmatrix} x_{21}^2 & y_{21}^2 & x_{21}y_{21} \\ x_{32}^2 & y_{32}^2 & x_{32}y_{32} \\ x_{13}^2 & y_{13}^2 & x_{13}y_{13} \end{bmatrix} \begin{bmatrix} \dfrac{\partial^2 w}{\partial x^2} \\ \dfrac{\partial^2 w}{\partial y^2} \\ 2\dfrac{\partial^2 w}{\partial x \partial y} \end{bmatrix} = \mathbf{T}^{-1}\boldsymbol{\kappa}, \tag{26.14}$$

the inverse of which is

$$\boldsymbol{\kappa} = \begin{bmatrix} \dfrac{\partial^2 w}{\partial x^2} \\ \dfrac{\partial^2 w}{\partial y^2} \\ 2\dfrac{\partial^2 w}{\partial x \partial y} \end{bmatrix} = \frac{1}{4A^2} \begin{bmatrix} y_{23}y_{13} & y_{31}y_{21} & y_{12}y_{32} \\ x_{23}x_{13} & x_{31}x_{21} & x_{12}x_{32} \\ y_{23}x_{31} + x_{32}y_{13} & y_{31}x_{12} + x_{13}y_{21} & y_{12}x_{23} + x_{21}y_{32} \end{bmatrix} \begin{bmatrix} \dfrac{\partial^2 w}{\partial \pi_{21}^2} \\ \dfrac{\partial^2 w}{\partial \pi_{32}^2} \\ \dfrac{\partial^2 w}{\partial \pi_{13}^2} \end{bmatrix} = \mathbf{T}\boldsymbol{\chi}. \tag{26.15}$$

The transformation equations (26.14) and (26.15) are assumed to hold even if $w(x, y)$ is only known in a weak sense.

§26.A.2. The Basic Stiffness Template

Following Militello and Felippa [20] the α-parametrized basic stiffness is defined as the linear combination

$$\mathbf{K}_b = A^{-1}\mathbf{L}\mathbf{D}\mathbf{L}^T, \qquad \mathbf{L} = (1-\alpha)\mathbf{L}_l + \alpha\mathbf{L}_q \tag{26.16}$$

where $\mathbf{L}$ is a force-lumping matrix that maps an internal constant moment field to node forces. $\mathbf{L}_l$ and $\mathbf{L}_q$ are called the linear and quadratic versions, respectively, of $\mathbf{L}$:

$$\mathbf{L}_l^T = \begin{bmatrix} 0 & 0 & y_{32} & 0 & 0 & y_{13} & 0 & 0 & y_{21} \\ 0 & x_{32} & 0 & 0 & x_{13} & 0 & 0 & x_{21} & 0 \\ 0 & y_{23} & x_{23} & 0 & y_{31} & x_{31} & 0 & y_{12} & x_{12} \end{bmatrix} \tag{26.17}$$

$$\mathbf{L}_q = \begin{bmatrix} c_{n21}s_{n21} - c_{n13}s_{n13} & -c_{n21}s_{n21} + c_{n13}s_{n13} & -(c_{n21}^2 - s_{n21}^2) + (c_{n13}^2 - s_{n13}^2) \\ \frac{1}{2}(c_{n21}^2 x_{12} + c_{n13}^2 x_{31}) & \frac{1}{2}(s_{n21}^2 x_{12} + s_{n13}^2 x_{31}) & s_{n21}^2 y_{21} + s_{n13}^2 y_{13} \\ -\frac{1}{2}(c_{n21}^2 y_{21} + c_{n13}^2 y_{13}) & -\frac{1}{2}(s_{n21}^2 y_{21} + s_{n13}^2 y_{13}) & -c_{n21}^2 x_{12} - s_{n13}^2 x_{31} \\ c_{n32}s_{n32} - c_{n21}s_{n21} & -c_{n32}s_{n32} + c_{n21}s_{n21} & -(c_{n32}^2 - s_{n32}^2) + (c_{n21}^2 - s_{n21}^2) \\ \frac{1}{2}(c_{n32}^2 x_{23} + c_{n21}^2 x_{12}) & \frac{1}{2}(s_{n32}^2 x_{23} + s_{n21}^2 x_{12}) & s_{n32}^2 y_{32} + s_{n21}^2 y_{21} \\ -\frac{1}{2}(c_{n32}^2 y_{32} + c_{n21}^2 y_{21}) & -\frac{1}{2}(s_{n32}^2 y_{32} + s_{n21}^2 y_{21}) & -c_{n32}^2 x_{23} - s_{n21}^2 x_{12} \\ c_{n13}s_{n13} + c_{n32}s_{n32} & -c_{n13}s_{n13} - c_{n32}s_{n32} & -(c_{n13}^2 - s_{n13}^2) + (c_{n32}^2 - s_{n32}^2) \\ \frac{1}{2}(c_{n13}^2 x_{31} + c_{n32}^2 x_{23}) & \frac{1}{2}(s_{n13}^2 x_{31} + s_{n32}^2 x_{23}) & s_{n13}^2 y_{13} + s_{n32}^2 y_{32} \\ -\frac{1}{2}(c_{n13}^2 y_{13} + c_{n32}^2 y_{32}) & -\frac{1}{2}(s_{n13}^2 y_{13} + s_{n32}^2 y_{32}) & -c_{n13}^2 x_{31} - s_{n32}^2 x_{23} \end{bmatrix} \tag{26.18}$$

Here c_{nji} and s_{nji} denote the cosine and sine, respectively, of the angle formed by x and the exterior normal to side $i \to j$.

Matrix $\mathbf{L}_l$ was introduced by Bergan and Nygård [13] and $\mathbf{L}_q$ by Militello and Felippa [20].

§26.A.3. The Higher Order Stiffness Template

For an element of constant $\mathbf{D}$, the higher order stiffness template is defined by

$$\mathbf{K}_h = \frac{A}{3}(\mathbf{B}_4^T\mathbf{D}_\chi\mathbf{B}_4 + \mathbf{B}_5^T\mathbf{D}_\chi\mathbf{B}_5 + \mathbf{B}_6^T\mathbf{D}_\chi\mathbf{B}_6) \tag{26.19}$$

where $\mathbf{D}_\chi = \mathbf{T}^T\mathbf{D}\mathbf{T}$ is the plate constitutive relation expressed in terms of natural curvatures and moments, and $\mathbf{B}_{\chi m}$ are the natural curvature-displacement matrices evaluated at the midpoints $m = 4, 5, 6$ opposing corners 3,1,2, respectively.

These matrices are parametrized as follows. Define the geometric invariants

$$\lambda_1 = \frac{x_{12}x_{13} + y_{12}y_{13}}{x_{21}^2 + y_{21}^2} - \tfrac{1}{2}, \quad \lambda_2 = \frac{x_{23}x_{21} + y_{23}y_{21}}{x_{32}^2 + y_{32}^2} - \tfrac{1}{2}, \quad \lambda_3 = \frac{x_{31}x_{32} + y_{31}y_{32}}{x_{13}^2 + y_{13}^2} - \tfrac{1}{2}. \tag{26.20}$$

These have a simple physical meaning as measures of triangle distortion (for an equilateral triangle, $\lambda_1 = \lambda_2 = \lambda_3 = 0$). In the following expressions, the β-derived coefficients γ_i and σ_i are selected so that the $\mathbf{B}_{\chi m}$ matrices are exactly orthogonal to all rigid body modes and constant curvature states. This is a requirement of the fundamental stiffness decomposition.

$$\begin{aligned}
&\beta_1 = \beta_{10}+\beta_{11}\lambda_3+\beta_{12}\lambda_1+\beta_{13}\lambda_2,\ \ \beta_2 = \beta_{20}+\beta_{21}\lambda_3+\beta_{22}\lambda_1+\beta_{23}\lambda_2,\ \ \beta_3 = \beta_{30}+\beta_{31}\lambda_3+\beta_{32}\lambda_1+\beta_{33}\lambda_2,\\
&\beta_4 = \beta_{40}+\beta_{41}\lambda_3+\beta_{42}\lambda_1+\beta_{43}\lambda_2,\ \ \beta_5 = \beta_{50}+\beta_{51}\lambda_3+\beta_{52}\lambda_1+\beta_{53}\lambda_2,\ \ \beta_6 = \beta_{60}+\beta_{61}\lambda_3+\beta_{62}\lambda_1+\beta_{63}\lambda_2,\\
&\beta_7 = \beta_{70}+\beta_{71}\lambda_3+\beta_{72}\lambda_1+\beta_{73}\lambda_2,\ \ \beta_8 = \beta_{80}+\beta_{81}\lambda_3+\beta_{82}\lambda_1+\beta_{83}\lambda_2,\ \ \beta_9 = \beta_{90}+\beta_{91}\lambda_3+\beta_{92}\lambda_1+\beta_{93}\lambda_2,\\
&\gamma_1 = \beta_1 + \beta_3,\ \gamma_2 = \beta_3,\ \gamma_3 = \beta_2 + \beta_3,\ \gamma_4 = \beta_4 + \beta_9,\ \gamma_5 = \beta_9,\ \gamma_6 = \beta_6 + \beta_8,\\
&\gamma_7 = \beta_6 + \beta_7,\ \gamma_8 = \beta_6,\ \gamma_9 = \beta_5 + \beta_9,\ \sigma_1 = 2\gamma_3 - 2\gamma_1,\ \sigma_2 = 2\gamma_1,\ \sigma_3 = 2\gamma_3,\\
&\sigma_4 = 2\gamma_9 - 2\gamma_4,\ \sigma_5 = 2\gamma_4,\ \sigma_6 = -2\gamma_6,\ \sigma_7 = 2\gamma_6 - 2\gamma_7,\ \sigma_8 = 2\gamma_7,\ \sigma_9 = -2\gamma_9
\end{aligned}$$

$$\mathbf{B}_{\chi 4} = \begin{bmatrix} \sigma_5 & \gamma_4 y_{31} + \gamma_5 y_{23} & \gamma_4 x_{13} + \gamma_5 x_{32} & \sigma_9 & \beta_9 y_{31} + \gamma_9 y_{23} & \beta_9 x_{13} + \gamma_9 x_{32} & \sigma_4 & \beta_4 y_{31} + \beta_5 y_{23} & \beta_4 x_{13} + \beta_5 x_{32} \\ \sigma_8 & \gamma_7 y_{31} + \gamma_8 y_{23} & \gamma_7 x_{13} + \gamma_8 x_{32} & \sigma_6 & \beta_6 y_{31} + \gamma_6 y_{23} & \beta_6 x_{13} + \gamma_6 x_{32} & \sigma_7 & \beta_7 y_{31} + \beta_8 y_{23} & \beta_7 x_{13} + \beta_8 x_{32} \\ \sigma_2 & \gamma_1 y_{31} + \gamma_2 y_{23} & \gamma_1 x_{13} + \gamma_2 x_{32} & \sigma_3 & \beta_3 y_{31} + \gamma_3 y_{23} & \beta_3 x_{13} + \gamma_3 x_{32} & \sigma_1 & \beta_1 y_{31} + \beta_2 y_{23} & \beta_1 x_{13} + \beta_2 x_{32} \end{bmatrix} \tag{26.21}$$

$$\begin{aligned}
&\beta_1 = \beta_{10}+\beta_{11}\lambda_1+\beta_{12}\lambda_2+\beta_{13}\lambda_3,\ \ \beta_2 = \beta_{20}+\beta_{21}\lambda_1+\beta_{22}\lambda_2+\beta_{23}\lambda_3,\ \ \beta_3 = \beta_{30}+\beta_{31}\lambda_1+\beta_{32}\lambda_2+\beta_{33}\lambda_3,\\
&\beta_4 = \beta_{40}+\beta_{41}\lambda_1+\beta_{42}\lambda_2+\beta_{43}\lambda_3,\ \ \beta_5 = \beta_{50}+\beta_{51}\lambda_1+\beta_{52}\lambda_2+\beta_{53}\lambda_3,\ \ \beta_6 = \beta_{60}+\beta_{61}\lambda_1+\beta_{62}\lambda_2+\beta_{63}\lambda_3,\\
&\beta_7 = \beta_{70}+\beta_{71}\lambda_1+\beta_{72}\lambda_2+\beta_{73}\lambda_3,\ \ \beta_8 = \beta_{80}+\beta_{81}\lambda_1+\beta_{82}\lambda_2+\beta_{83}\lambda_3,\ \ \beta_9 = \beta_{90}+\beta_{91}\lambda_1+\beta_{92}\lambda_2+\beta_{93}\lambda_3,\\
&\gamma_1 = \beta_1 + \beta_3,\ \gamma_2 = \beta_3,\ \gamma_3 = \beta_2 + \beta_3,\ \gamma_4 = \beta_4 + \beta_9,\ \gamma_5 = \beta_9,\ \gamma_6 = \beta_6 + \beta_8,\\
&\gamma_7 = \beta_6 + \beta_7,\ \gamma_8 = \beta_6,\ \gamma_9 = \beta_5 + \beta_9,\ \sigma_1 = 2\gamma_3 - 2\gamma_1,\ \sigma_2 = 2\gamma_1,\ \sigma_3 = -2\gamma_3,\\
&\sigma_4 = 2\gamma_9 - 2\gamma_4,\ \sigma_5 = 2\gamma_4,\ \sigma_6 = -2\gamma_6,\ \sigma_7 = 2\gamma_6 - 2\gamma_7,\ \sigma_8 = 2\gamma_7,\ \sigma_9 = -2\gamma_9
\end{aligned}$$

$$\mathbf{B}_{\chi 5} = \begin{bmatrix} \sigma_1 & \beta_1 y_{12} + \beta_2 y_{31} & \beta_1 x_{21} + \beta_2 x_{13} & \sigma_2 & \gamma_1 y_{12} + \gamma_2 y_{31} & \gamma_1 x_{21} + \gamma_2 x_{13} & \sigma_3 & \beta_3 y_{12} + \gamma_3 y_{31} & \beta_3 x_{21} + \gamma_3 x_{13} \\ \sigma_4 & \beta_4 y_{12} + \beta_5 y_{31} & \beta_4 x_{21} + \beta_5 x_{13} & \sigma_5 & \gamma_4 y_{12} + \gamma_5 y_{31} & \gamma_4 x_{21} + \gamma_5 x_{13} & \sigma_9 & \beta_9 y_{12} + \gamma_9 y_{31} & \beta_9 x_{21} + \gamma_9 x_{13} \\ \sigma_7 & \beta_7 y_{12} + \beta_8 y_{31} & \beta_7 x_{21} + \beta_8 x_{13} & \sigma_8 & \gamma_7 y_{12} + \gamma_8 y_{31} & \gamma_7 x_{21} + \gamma_8 x_{13} & \sigma_6 & \beta_6 y_{12} + \gamma_6 y_{31} & \beta_6 x_{21} + \gamma_6 x_{13} \end{bmatrix} \tag{26.22}$$

$$
\begin{aligned}
&\beta_1 = \beta_{10}+\beta_{11}\lambda_2+\beta_{12}\lambda_3+\beta_{13}\lambda_1,\ \ \beta_2 = \beta_{20}+\beta_{21}\lambda_2+\beta_{22}\lambda_3+\beta_{23}\lambda_1,\ \ \beta_3 = \beta_{30}+\beta_{31}\lambda_2+\beta_{32}\lambda_3+\beta_{33}\lambda_1,\\
&\beta_4 = \beta_{40}+\beta_{41}\lambda_2+\beta_{42}\lambda_3+\beta_{43}\lambda_1,\ \ \beta_5 = \beta_{50}+\beta_{51}\lambda_2+\beta_{52}\lambda_3+\beta_{53}\lambda_1,\ \ \beta_6 = \beta_{60}+\beta_{61}\lambda_2+\beta_{62}\lambda_3+\beta_{63}\lambda_1,\\
&\beta_7 = \beta_{70}+\beta_{71}\lambda_2+\beta_{72}\lambda_3+\beta_{73}\lambda_1,\ \ \beta_8 = \beta_{80}+\beta_{81}\lambda_2+\beta_{82}\lambda_3+\beta_{83}\lambda_1,\ \ \beta_9 = \beta_{90}+\beta_{91}\lambda_2+\beta_{92}\lambda_3+\beta_{93}\lambda_1,\\
&\gamma_1 = \beta_1+\beta_3,\ \gamma_2 = \beta_3,\ \gamma_3 = \beta_2+\beta_3,\ \gamma_4 = \beta_4+\beta_9,\ \gamma_5 = \beta_9,\ \gamma_6 = \beta_6+\beta_8,\\
&\gamma_7 = \beta_6+\beta_7,\ \gamma_8 = \beta_6,\ \gamma_9 = \beta_5+\beta_9,\ \sigma_1 = 2\gamma_3-2\gamma_1,\ \sigma_2 = 2\gamma_1,\ \sigma_3 = -2\gamma_3,\\
&\sigma_4 = 2\gamma_9-2\gamma_4,\ \sigma_5 = 2\gamma_4,\ \sigma_6 = -2\gamma_6,\ \sigma_7 = 2\gamma_6-2\gamma_7,\ \sigma_8 = 2\gamma_7,\ \sigma_9 = -2\gamma_9
\end{aligned}
$$

$$
\mathbf{B}_{\chi 6} = \begin{bmatrix}
\sigma_6 & \beta_6 y_{23}+\gamma_6 y_{12} & \beta_6 x_{32}+\gamma_6 x_{21} & \sigma_7 & \beta_7 y_{23}+\beta_8 y_{12} & \beta_7 x_{32}+\beta_8 x_{21} & \sigma_8 & \gamma_7 y_{23}+\gamma_8 y_{12} & \gamma_7 x_{32}+\gamma_8 x_{21}\\
\sigma_3 & \beta_3 y_{23}+\gamma_3 y_{12} & \beta_3 x_{32}+\gamma_3 x_{21} & \sigma_1 & \beta_1 y_{23}+\beta_2 y_{12} & \beta_1 x_{32}+\beta_2 x_{21} & \sigma_2 & \gamma_1 y_{23}+\gamma_2 y_{12} & \gamma_1 x_{32}+\gamma_2 x_{21}\\
\sigma_9 & \beta_9 y_{23}+\gamma_9 y_{12} & \beta_9 x_{32}+\gamma_9 x_{21} & \sigma_4 & \beta_4 y_{23}+\beta_5 y_{12} & \beta_4 x_{32}+\beta_5 x_{21} & \sigma_5 & \gamma_4 y_{23}+\gamma_5 y_{12} & \gamma_4 x_{32}+\gamma_5 x_{21}
\end{bmatrix} \tag{26.23}
$$

Equations (26.19) through (26.23) complete the definition of the KPT-1-36 template.